


Nonequilibrium correlation dynamics in the one-dimensional Fermi-Hubbard model: A testbed for the two-particle reduced density matrix theory

Stefan Donsa,¹ Fabian Lackner ¹, Joachim Burgdörfer,¹ Michael Bonitz ^{2,3}, Benedikt Kloss,⁴
Angel Rubio,^{5,4} and Iva Březinová ^{1,4,*}

¹*Institute for Theoretical Physics, Vienna University of Technology, Wiedner Hauptstraße 8-10/136, 1040 Vienna, Austria, EU*

²*Institut für Theoretische Physik und Astrophysik, Christian-Albrechts-Universität zu Kiel, D-24098 Kiel, Germany, EU*

³*Kiel Nano, Surface and Interface Science KiNSIS, Kiel University, Germany, EU*

⁴*Center for Computational Quantum Physics (CCQ), Flatiron Institute, New York, New York, USA*

⁵*Max Planck Institute for the Structure and Dynamics of Matter, Hamburg, Germany, EU*



(Received 21 February 2023; revised 16 May 2023; accepted 19 May 2023; published 12 July 2023)

We explore the nonequilibrium dynamics of a one-dimensional Fermi-Hubbard system as a sensitive testbed for the capabilities of the time-dependent two-particle reduced density matrix (TD2RDM) theory to accurately describe time-dependent correlated systems. We follow the time evolution of the out-of-equilibrium finite-size Fermi-Hubbard model initialized by a quench over extended periods of time. By comparison with exact calculations for small systems and with matrix product state calculations for larger systems but limited to short times, we demonstrate that the TD2RDM theory can accurately account for the nonequilibrium dynamics in the regime from weak to moderately strong interparticle correlations. We find that the quality of the approximate reconstruction of the three-particle cumulant (or correlation) required for the closure of the equations of motion for the reduced density matrix is key to the accuracy of the numerical TD2RDM results. We identify the size of the dynamically induced three-particle correlations and the amplitude of cross correlations between the two- and three-particle cumulants as critical parameters that control the accuracy of the TD2RDM theory when current state-of-the-art reconstruction functionals are employed.

DOI: [10.1103/PhysRevResearch.5.033022](https://doi.org/10.1103/PhysRevResearch.5.033022)

I. INTRODUCTION

Accurately describing the correlated out-of-equilibrium dynamics of interacting many-particle systems has remained a great challenge to date. Frequent realizations of such out-of-equilibrium dynamics involve either quenches and relaxation of initially prepared excited states of systems governed by a time-independent Hamiltonian, or systems driven by an explicitly time-dependent Hamiltonian. Such systems are at the forefront of current experimental and theoretical studies (see, e.g., Refs. [1–14]). Several recent experiments have shown that exotic states of matter can be generated by ultrashort pulses of external fields or energetic ions and that relaxation and decoherence can be strongly influenced by interparticle correlations [15–23].

A versatile method to reliably describe the nonequilibrium scenarios of correlated many-body systems, in particular in extended systems and for extended periods of time, is still lacking. Direct many-body wave-function-based methods can be applied only to systems with a moderate number

of degrees of freedom and pure states as they eventually face the exponential wall of computational effort when increasing the number of particles and the time interval of propagation [2,9,24,25]. Application of the time-dependent density matrix renormalization group (DMRG) theory [2,26] has been shown to yield numerically accurate results, currently, however, limited to one-dimensional (1D) systems and short time scales (see, e.g., Refs. [27–29]). Similarly, the closely related time-dependent matrix product state (MPS) method [25,30] invoking the time-dependent variational principle, is also limited to small propagation times for mesoscopic system sizes of a few tens of particles (see, e.g., Ref. [31]) with the increasing bond dimension as a function of time as the major bottleneck (see, e.g., Ref. [32]).

The multidimensionally distributed complex information encoded in the quantum many-body wave function is, however, often not needed for the extraction of many physical observables. Therefore, an appealing alternative are time-dependent quantum many-body methods that attempt to bypass the use of the many-body wave function altogether. Upon successively tracing out more and more degrees of freedom, information and complexity is lost but, in turn, the reduced system is rendered increasingly tractable.

A well-known limit of this reduction is the time-dependent particle density $n(\mathbf{r}, t)$. The corresponding many-body theory, the time-dependent density functional theory (TDDFT) [33,34] with the Kohn-Sham ansatz features a linear scaling with particle number and remains to date the

*iva.brezinova@tuwien.ac.at

Published by the American Physical Society under the terms of the [Creative Commons Attribution 4.0 International](https://creativecommons.org/licenses/by/4.0/) license. Further distribution of this work must maintain attribution to the author(s) and the published article's title, journal citation, and DOI.

only time-dependent quantum many-body theory applicable to large extended systems with weak correlations. Its major drawback, however, is the fundamental lack of knowledge of the exact exchange-correlation (XC) functional. The pathway towards systematic improvements beyond the currently frequently used approximate adiabatic XC functionals is still a widely open question and the applicability of TDDFT to correlated systems is limited. Alternatively, the so-called time-dependent current-density functional theory has been proposed for which, up to now, however, only few approximations for the exchange-correlation vector potential have become available [35–37].

Going up one step of the ladder of reduction the one-particle reduced density matrix (1RDM) $D_1(\mathbf{r}_1, \mathbf{r}'_1, t)$ allows one to avoid some of the problems of TDDFT [38–40] while facing others. The equation of motion for the 1RDM corresponds to the first equation within the Bogoliubov-Born-Green-Kirkwood-Yvon (BBGKY) hierarchy [41,42] and thus couples the 1RDM to the two-particle reduced density matrix (2RDM), $D_{12}(\mathbf{r}_1, \mathbf{r}_2, \mathbf{r}'_1, \mathbf{r}'_2, t)$. Closing the equations of motion requires representing the 2RDM as a functional of the 1RDM, which is challenging in the presence of medium to strong correlations and for time-dependent settings.

An alternative route to an accurate description of nonequilibrium correlated quantum many-body systems involves nonequilibrium Green's function (NEGF) methods, going back to the pioneering work of Keldysh [43]. They have been applied to a wide range of physical systems (see, e.g., Refs. [44,45] and references therein) but are impeded by a nonlinear time scaling, which has only recently been overcome [29,46–48]. Moreover, they exhibit a similar hierarchical coupling between different orders of Green's functions, which is subject to closure approximations as in the case of reduced density matrices (see, e.g., Refs. [44]).

The importance of two-particle correlations as imprinted by the pairwise interaction potentials in most physical systems calls for the use of the 2RDM itself as the fundamental object for representing the many-body system. When only one- and two-body operators are present in the Hamiltonian, the total energy of the system can be exactly expressed in terms of the 2RDM. The fact that the energy is an exactly known functional of the 2RDM has been meanwhile exploited in numerous calculations of ground-state energies in quantum many-body systems [49–53].

In this paper we investigate the time-dependent 2RDM. The equation of motion for propagating the 2RDM of an excited system, the second equation of motion the BBGKY hierarchy, requires, the knowledge of the three-particle reduced density matrix (3RDM). Many important works have been devoted in the past to develop reconstruction functionals of the 3RDM in terms of the 2RDM for the quantum many-body ground-state problem [54–60]. Incorporating such reconstruction functionals into the time-dependent setting within the time-dependent 2RDM method (TD2RDM), we have recently succeeded in calculating the dynamics of multielectron atoms driven by strong laser fields [61,62]. Motivated by the stability and remarkable accuracy of this method, it is the aim of the present paper to explore the application of the TD2RDM theory to extended systems, and to systems featuring stronger correlations than typically present in multielectron atoms.

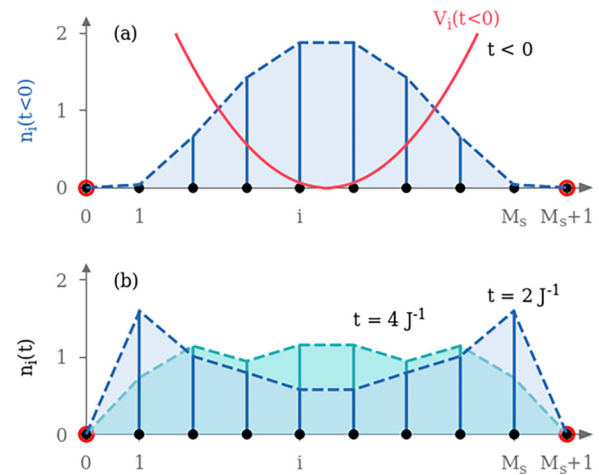


FIG. 1. Fermi-Hubbard model with M_s sites initially ($t < 0$) confined by an external harmonic potential. Dirichlet (hard-wall) boundary conditions are imposed on site 0 and $M_s + 1$ marked by red circles. (a) The one-particle site-occupation numbers n_i of the initial ground state in the potential, which represents an excitation of the potential-free Fermi-Hubbard model after the quench. (b) Snapshots of the time evolved $n_i(t)$ at $t = 2J^{-1}$ and $t = 4J^{-1}$. The parameters used are $V = J$ and $U = J$.

A paradigmatic model system for this endeavor is the Fermi-Hubbard model due to its structural simplicity and the one-parameter tunability from weakly to strongly correlated dynamics. Moreover, this model system can nowadays be realized and accurately probed with ultracold atoms in optical lattices even with single-site resolution (see, e.g., Refs. [63–69] and references therein) and is, of course, of conceptual relevance for the study of correlated quantum matter in real solids. Several state-of-the-art methods have been tested by application to the Fermi-Hubbard model. They include the NEGF methods [16,28,70], as well as approaches based on Green's functions exploiting the mapping between the Fermi-Hubbard model and an impurity model where the impurity is treated in a fully correlated fashion and is coupled to an external uncorrelated bath. These methods, such as time-dependent dynamical mean-field theory [6] or the explicit sum of a high-order perturbation series in the interaction on the Keldysh contour using quantum Monte Carlo methods [71–73] have the advantage that extended systems can be treated through the coupling of the impurity to an extended bath. However, correlations between distant sites are not well represented.

As a prototypical example, we apply the TD2RDM theory to the dynamics of the Fermi-Hubbard model at half-filling initialized by a quench, i.e., by suddenly switching off a confining potential that prepares the initial out-of-equilibrium state (Fig. 1). In order to test and to benchmark the TD2RDM we consider in the present work 1D systems with a relatively small number of sites. For these systems a detailed assessment of the accuracy by comparison with numerically exact or highly accurate solutions is still possible allowing us to perform large and systematic parameter scans over many different interaction strengths and excitation energies. We generate (nearly) exact solutions by either direct propagation

of the Schrödinger equation or using highly accurate matrix product state (MPS) calculations within the time-dependent variational principle [25,30,31]. We follow the dynamics over relatively long times (≥ 50 in units of the inverse hopping amplitude) and study the exact buildup of dynamical correlations, which can give valuable hints for the applicability of the TD2RDM method as well as for the improvements of reconstruction functionals. We emphasize that our present restriction to 1D systems and to moderate sizes is due to the difficulty of obtaining exact or highly accurate results for comparison, rather than due to the limitations of the TD2RDM theory itself. The latter can be easily extended to larger systems and higher dimensions without encountering major complications. We also compare with time-dependent Hartree-Fock (TDHF) predictions to access the influence of two-particle correlations neglected by mean-field theories. We analyze the accuracy of the TD2RDM theory as a function of the strength of the interparticle interaction as well as of the degree of initial excitation. One focus is on detailed probes of the accuracy of the time-dependent three-particle correlations resulting from different state-of-the-art reconstruction functionals.

The structure of the paper is as follows: In Sec. II we briefly present the model system under investigation, the one-dimensional Fermi-Hubbard model at half-filling. The key ingredients of the TD2RDM theory are reviewed in Sec. III. We numerically analyze the dynamics of two- and three-particle correlations, the so-called cumulants, which are the key ingredient to reconstruction functionals, for small systems by comparison with exact calculations in Sec. IV. Fully self-consistent TD2RDM simulations for the time evolution of the out-of-equilibrium dynamics as monitored by the one-site occupation number are presented in Sec. V, followed by concluding remarks and an outlook to future improvements in Sec. VI. As units we use $\hbar = m = e = 1$ unless otherwise stated.

II. OUT-OF-EQUILIBRIUM FERMI-HUBBARD MODEL

We consider a 1D chain with a number of M_s sites (Fig. 1) and impose Dirichlet boundary conditions (i.e., hard-wall boundary conditions) at sites 0 and $M_s + 1$. These two sites remain unoccupied during the time evolution. The present choice of boundary conditions is motivated by typical quantum simulator experiments with trapped ultracold atoms (see, e.g., Ref. [74]). Other boundary conditions, such as periodic boundary conditions, could be easily implemented as well without requiring major changes of the present analysis. The Hamiltonian of the Fermi-Hubbard model in the presence of an external potential initializing the quench is given in second quantization by

$$H = -J \sum_{\langle i,j \rangle} \sum_{\sigma} a_{i\sigma}^{\dagger} a_{j\sigma} + U \sum_i n_i^{\uparrow} n_i^{\downarrow} + \sum_{i,\sigma} V_i(t) a_{i\sigma}^{\dagger} a_{i\sigma}, \quad (1)$$

where $\langle i, j \rangle$ denotes nearest-neighbor hopping, J the hopping amplitude, $a_{i\sigma}^{(\dagger)}$ the one-particle annihilation (creation) operators, $n_i^{\uparrow(\downarrow)} = a_{i\uparrow(\downarrow)}^{\dagger} a_{i\uparrow(\downarrow)}$, the occupation number operators for

particles with spin up (down) at site i , U the strength of on-site interaction controlling the correlation energy in the system. $V_i(t)$ is the explicitly time-dependent potential chosen to be harmonic in the present case,

$$V_i(t) = \theta(-t) \frac{V^2}{2} \left(i - \frac{M_s + 1}{2} \right)^2, \quad (2)$$

which determines the initial excited state (the ground state of H in the potential for $t < 0$), and induces the dynamics by a sudden potential quench at $t = 0$. We consider in the following the spin-symmetric Fermi-Hubbard system at half filling, i.e., particle number $N = M_s$ and the number of spin-up particles equals to the number of spin-down particles (total spin-singlet case).

Figure 1 illustrates the quench-induced dynamics on the level of the one-particle site-occupation numbers n_i corresponding to the diagonal elements of the one-particle reduced density matrix D_1 . The ground state of the interacting many-body system in the potential [Fig. 1(a)] represents an excited state of the field-free Fermi-Hubbard system and, thus, an out-of-equilibrium state that evolves in time after the quench [Fig. 1(b)]. We explore in the following within the framework of TD2RDM theory the importance of interparticle correlations induced by U [Eq. (1)] in both the stationary initial state as well the time-dependent correlations induced by the sudden quench.

III. OUTLINE OF TD2RDM THEORY

A. Equation of motion

The central object of our method is the 2RDM, which results from the exact pure N -body wave function $|\Psi(t)\rangle$ by tracing out all but two particles. We refer to the 2RDM in a basis-independent notation as D_{12} . It follows from $|\Psi(t)\rangle$ as

$$D_{12}(t) = N(N-1) \text{Tr}_{3\dots N} |\Psi(t)\rangle \langle \Psi(t)|, \quad (3)$$

with N the number of particles, $N(N-1)$ the normalization related to particles pairs, and $\text{Tr}_{3\dots N}$ indicating the tracing out of all particles except for the two particles 1 and 2 of interest. More generally, the pRDM is obtained from

$$D_{1\dots p}(t) = \frac{N!}{(N-p)!} \text{Tr}_{p+1\dots N} |\Psi(t)\rangle \langle \Psi(t)|, \quad (4)$$

with normalization factor $N!/(N-p)!$.

The equation of motion of the 2RDM corresponds to the second equation within the BBGKY hierarchy and reads

$$i\partial_t D_{12}(t) = [h_1 + h_2 + W_{12}, D_{12}] + \text{Tr}_3 [W_{13} + W_{23}, D_{123}], \quad (5)$$

where the square brackets denote commutators. The Hamiltonian governing Eq. (5) is given (in first quantization) by

$$H = \sum_{n=1}^N h_n + \sum_{n<m}^N W_{nm}, \quad (6)$$

where h_n is the single-particle Hamilton operator, and W_{nm} the two-particle interaction operator. In a basis of spin orbitals $\{|\psi_{i\sigma}\rangle\}_{i=1}^{M_s}$ with $\sigma = \uparrow$ or $\sigma = \downarrow$ localized at a single site i (given, e.g., by s-wave orbitals localized at atomic sites in

solids or potential minima in optical lattices of ultracold atoms) the terms in Eq. (6) yield the explicit matrix representation for the nearest-neighbor hopping as

$$h_{j\sigma}^{i\sigma'} = \langle \psi_{i\sigma'} | h_1 | \psi_{j\sigma} \rangle = -J\delta_j^{i+1}\delta_{\sigma}^{\sigma'} - J\delta_j^{i-1}\delta_{\sigma}^{\sigma'}, \quad (7)$$

and the on-site interaction of particles with different spins as

$$W_{j_1\sigma_1 j_2\sigma_2}^{i_1\sigma_1' i_2\sigma_2'} = \langle \psi_{i_1\sigma_1'} \psi_{i_2\sigma_2'} | W_{12} | \psi_{j_1\sigma_1} \psi_{j_2\sigma_2} \rangle \\ = U\delta_{j_1}^{i_1}\delta_{j_2}^{i_2}\delta_{j_1,j_2}\delta_{\sigma_1}^{\sigma_1'}\delta_{\sigma_2}^{\sigma_2'}(1 - \delta_{\sigma_1,\sigma_2}). \quad (8)$$

For any initial state (pure or mixed) described by $D_{12}(t=0)$, Eq. (5) allows us to propagate the 2RDM without any knowledge of the many-body wave function $|\Psi(t)\rangle$. However, since all equations of the BBGKY hierarchy couple to the density matrix of the next higher order, propagation of the 2RDM requires closure, i.e., a sufficiently accurate representation of the 3RDM (in the following called reconstruction) in terms of the 2RDM. Closure of the equations of motion by reconstruction (denoted by the superscript R in the following) of the 3RDM by the 2RDM, i.e.,

$$D_{123} \approx D_{123}^R[D_{12}] \quad (9)$$

poses thus a major challenge for the implementation of the TD2RDM theory as a useful and accurate computational tool. In the spirit of a quantum Boltzmann transport equation [41], we call the term in Eq. (5) containing the D_{123} the collision operator (or collision integral) C ,

$$C[D_{123}] = \text{Tr}_3[W_{13} + W_{23}, D_{123}]. \quad (10)$$

While for the collision operator an approximation to the reconstruction of the 3RDM is required, the time-dependent 2RDM, $D_{12}(t)$, fully includes all two-particle interactions and correlations without any additional approximation. The solutions of the equations of motion of the 2RDM [Eq. (5)] feature a direct relation to Green's functions, which opens the door to employ well-established diagrammatic methods also within the TD2RDM theory. The pRDMs can be identified with the equal-time limits of the p -particle Green's functions $G_{1\dots p}^<(t_1, \dots, t_p, t_1', \dots, t_p')$. For the 1RDM and 2RDM, e.g., we get (see, e.g., Refs. [29,44])

$$D_1(t) = -iG_1^<(t, t) \quad (11)$$

$$D_{12}(t) = i^2 G_{12}^<(t, t, t, t). \quad (12)$$

In a given single-particle basis $D_{12}(t)$ is represented by the matrix

$$D_{j_1\sigma_1 j_2\sigma_2}^{i_1\sigma_1' i_2\sigma_2'} = \langle \Psi(t) | a_{i_1\sigma_1'}^\dagger a_{i_2\sigma_2'}^\dagger a_{j_2\sigma_2} a_{j_1\sigma_1} | \Psi(t) \rangle. \quad (13)$$

Because of the dependence of C on D_{123} , the equation of motion of the 2RDM represented in a single-particle basis of dimension M scales as M^7 for a general pair interaction W . In the present spin-symmetric realization of the Fermi-Hubbard model with equal number of spin-up and spin-down particles, the complexity of the problem is considerably reduced. Given a total spin singlet state, the calculation of Eq. (5) can be reduced to that of the spin block $D_{j_1\uparrow j_2\downarrow}^{i_1\uparrow i_2\downarrow}$, which contains all the information on the entire $D_{12}(t)$ [61]. All other spin blocks can be obtained from this particular block either through trivial exchange or spin-flip symmetries, or through the following

relation:

$$D_{j_1\uparrow j_2\uparrow}^{i_1\uparrow i_2\uparrow} = D_{j_1\uparrow j_2\downarrow}^{i_1\uparrow i_2\downarrow} - D_{j_2\uparrow j_1\downarrow}^{i_1\uparrow i_2\downarrow}. \quad (14)$$

Correspondingly, only the 3RDM block $D_{j_1\uparrow j_2\uparrow j_3\downarrow}^{i_1\uparrow i_2\uparrow i_3\downarrow}$ needs to be constructed instead of the entire 3RDM. The equation of motion for $D_{j_1\uparrow j_2\downarrow}^{i_1\uparrow i_2\downarrow}$ is given in Appendix A. Due to the simple on-site interaction within the Fermi-Hubbard model [Eq. (8)], the equation of motion for the 2RDM scales as M_s^4 . For simplicity of notation, we drop the explicit spin labeling (\uparrow, \downarrow) unless specifically needed keeping in mind that only the spin blocks identified above need to be calculated.

B. Cumulant expansion

The pRDM describes, in general, the correlated dynamics of a p -tuple of particles embedded in a larger system, in particular in the pure state $|\Psi(t)\rangle$ of an N -particle system. In the absence of interparticle interactions, the pRDM reduces to the independent-particle limit where only Pauli exchange correlations via antisymmetrization are present. The pRDM can be expanded in term of correlators, in this context conventionally referred to as cumulants [75], of increasing order in the number of particles within the tuple to be correlated with each other.

For D_{12} the cumulant expansion reads

$$D_{12} = \hat{A}D_1D_2 + \Delta_{12} \quad (15)$$

with the two-particle cumulant (or correlator) Δ_{12} and \hat{A} the antisymmetrization operator acting on the two one-particle density matrices D_1 and D_2 . In the single-particle site representation

$$\hat{A}D_{j_1}^i D_{j_2}^i = D_{j_1}^i D_{j_2}^i - D_{j_2}^i D_{j_1}^i. \quad (16)$$

and Eq. (15) reads

$$D_{j_1 j_2}^{i_1 i_2} = \hat{A}D_{j_1}^{i_1} D_{j_2}^{i_2} + \Delta_{j_1 j_2}^{i_1 i_2}. \quad (17)$$

The cumulant expansion of D_{12} [Eq. (15)] can be diagrammatically visualized (Fig. 2). The key feature to be noted is that the cumulant expansion itself [Fig. 2(a)] does not invoke any ingredients from perturbation theory. The double lines represent the equal-time limit of the full one-particle propagator. The cumulant represents the sum over all connected diagrams between two one-particle propagators. For illustrative purposes and to connect to other theories we indicate in Figs. 2(b) and 2(c) the corresponding perturbative diagrammatic expansion of the constituents of Fig. 2(a), the one-particle propagator [Fig. 2(b)] and the two-particle cumulant [Fig. 2(c)]. We emphasize that within the TD2RDM theory the full 1RDM as well as the full 2RDM are included such that the use of the perturbation series [Figs. 2(b), 2(c)] can be avoided. However, these diagrammatic interrelations provide a helpful guidance for developing reconstruction functionals on the three-particle level.

The cumulant expansion of the 3RDM follows as

$$D_{123} = \hat{A}D_1D_2D_3 + \hat{A}\Delta_{12}D_3 + \Delta_{123}, \quad (18)$$

diagrammatically visualized in Fig. 3(a). The first term in Fig. 3(a) represents three uncorrelated particles, the second the contribution of two-particle correlations in the presence of a third uncorrelated particle, and the last the true three-particle

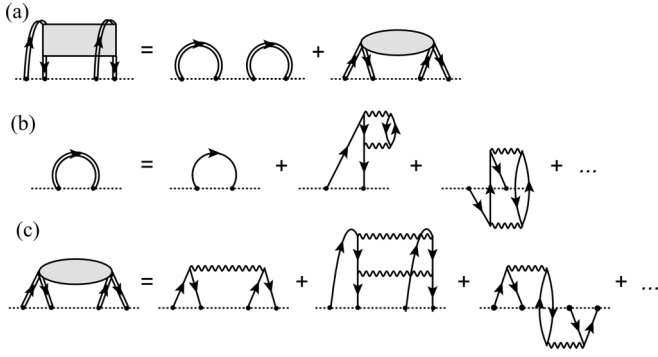


FIG. 2. (a) Diagrammatic representation of the 2RDM. The first term corresponds to $\hat{A}D_1D_2$ (the antisymmetrized contribution is not explicitly shown for brevity). The second term represents the cumulant Δ_{12} , which contains all connected diagrams between two single-particle propagators. Note that no perturbative expansion in the interparticle interaction W_{12} is involved in (a). (b) Diagrammatic perturbative expansion of D_1 , i.e., the equal-time limit of the full single-particle propagator. Two second-order diagrams in W_{12} (wavy lines) are shown as illustrative examples. The double line represents the full D_1 , while each single line in (b) and (c) stands for a Hartree-Fock propagator. (c) Diagrammatic perturbative expansion of the cumulant Δ_{12} with three prototypical diagrams to first and second order in W_{12} .

correlation or three-particle cumulant Δ_{123} containing all connected three-particle diagrams. For illustrative purposes we show also in Fig. 3(b) the first few low-order diagrams of a perturbative expansion of Δ_{123} in terms of Hartree-Fock propagators and pair interactions. We note again that the present TD2RDM theory does not make direct use of perturbation theory but we invoke the structure of these diagrams in the following to motivate the approximations of Δ_{123} in terms of one-particle propagators and two-particle cumulants.

C. Three-particle cumulant reconstruction

The challenge to render the TD2RDM theory operational is the closure of the equations of motion [Eq. (5)] by developing a reconstruction functional for the three-particle density matrix $D_{123}^R[D_{12}]$ [Eq. (9)]. The success of the TD2RDM method in describing the many-body dynamics relies on a sufficiently accurate approximation of this functional as has been shown for multielectron atoms [61,62]. While

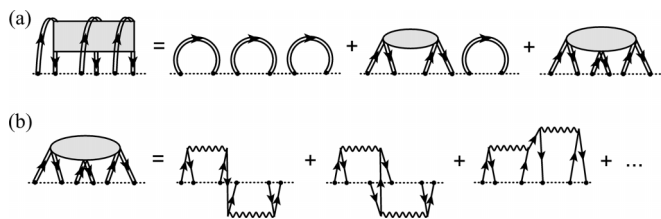


FIG. 3. (a) Diagrammatic representation of the 3RDM. The first term corresponds to $\hat{A}D_1D_2D_3$, the second corresponds to $\hat{A}\Delta_{12}D_3$, and the last to the three-particle cumulant Δ_{123} . The antisymmetrized contributions of each term are not shown for brevity. (b) Diagrammatic representation of the perturbative expansion of the three-particle cumulant, with several prototypical second-order connected diagrams ($\propto W_{12}^2$) shown.

for the nondegenerate ground state the existence of such a reconstruction is assured through Rosina’s theorem [76,77], it is presently unknown whether such an exact reconstruction also exists in a time-dependent setting. As Rosina’s theorem is an existence theorem, it does not lend itself to aid in the development of new functionals.

The cumulant expansion of D_{123} [Eq. (18)] reduces the task of finding a reconstruction functional to that of reconstructing the cumulant $\Delta_{123} = \Delta_{123}^R[D_{12}]$ as the other terms contributing to D_{123} are already known functionals of D_{12} (and D_1). Several approximate functionals $D_{123}^R[D_{12}]$ or $\Delta_{123}^R[D_{12}]$ have been recently proposed [54–56,59,60]. They provide the starting point of our analysis of the capability of the TD2RDM theory to capture nonequilibrium dynamics in correlated systems.

The simplest approximation to Δ_{123} attributed to Valdemoro (V) and coworkers [54] amounts to neglecting Δ_{123} altogether. Accordingly, the reconstruction functional becomes

$$D_{123}^V[D_{12}] = \hat{A}D_1D_2D_3 + \hat{A}\Delta_{12}D_3. \tag{19}$$

A similar approximation has been earlier investigated by Wang and Cassing [78]. Reconstruction functionals that include contributions from Δ_{123} and benchmarked in this paper have been derived from different perspectives but all rely on approximating Δ_{123} to second order in Δ_{12} . Nakatsuji and Yasuda (NY) [55] used diagrammatic techniques to arrive at

$$\Delta_{123}^{NY}[\Delta_{12}] = \hat{A}\Delta_{12}P_2\Delta_{23}, \tag{20}$$

where the intermediate single-particle projector P_i is given by

$$P_i = (3\Gamma_i - I_i - D_i)^{-1}, \tag{21}$$

with I_i the identity matrix, Γ_i a diagonal matrix in the eigenrepresentation of the 1RDM with eigenvalues 1 for the lowest N natural orbitals and zero otherwise. Γ_i is frequently (in ground-state calculations) referred to as the Hartree-Fock reference matrix. We note, however, that in the present context Γ_i refers to the natural orbitals of the nonperturbative 1RDM rather than to mean-field states. It has been shown [56] that this projector can be substantially simplified through an expansion in $\Gamma_i - D_i$, the zeroth order of which yields

$$P_i^{(0)} = (2\Gamma_i - I_i)^{-1}. \tag{22}$$

In practice, the summation over the index 2 in Eq. (20) is performed in the basis of natural orbitals with a matrix as the projector containing -1 for unoccupied and 1 for occupied orbitals. We have checked for all parameters U and V scanned in Sec. IV below that the difference between applying Eq. (21) vs. Eq. (22) is negligibly small [in regions where the NY + CC reconstruction has small errors, Eq. (22) even slightly outperforms Eq. (21)]. We therefore use the simpler approximation, Eq. (22). Thus, the NY reconstruction functional for D_{123} reads

$$D_{123}^{NY}[D_{12}] = D_{123}^V[D_{12}] + \Delta_{123}^{NY}[\Delta_{12}] = \hat{A}D_1D_2D_3 + \hat{A}\Delta_{12}D_3 + \Delta_{123}^{NY}[\Delta_{12}]. \tag{23}$$

Starting from a coupled-cluster ansatz for the wave function, a similar reconstruction functional has been derived by Tohyama and Schuck (TS) [59,60]. Including an empirically

found renormalization factor the TS reconstruction functional amounts to

$$\Delta_{123}^{\text{TS}} = \frac{1}{\mathcal{N}} \Delta_{123}^{\text{NY}}, \quad (24)$$

with renormalization factor $\mathcal{N} = 1 + \frac{1}{4} \text{Tr}_{12} |\Delta_{12}|^2$. The reconstruction functional thus reads

$$D_{123}^{\text{TS}}[D_{12}] = D_{123}^{\text{V}}[D_{12}] + \Delta_{123}^{\text{TS}}[\Delta_{12}]. \quad (25)$$

Mazziotti (M) devised a similar reconstruction of Δ_{123} along different lines starting from the cumulant decomposition of the 4RDM and assuming $\text{Tr}_4 \Delta_{1234} = 0$ with Δ_{1234} the four-particle cumulant [56,57]. This leads to an implicit equation for Δ_{123} , which can be explicitly solved in the eigenbasis of the 1RDM. Further details of this reconstruction functional are summarized in Appendix B. The corresponding reconstruction functional of the three-particle cumulant is denoted by Δ_{123}^{M} and the reconstructed three-particle density matrix by

$$D_{123}^{\text{M}}[D_{12}] = D_{123}^{\text{V}}[D_{12}] + \Delta_{123}^{\text{M}}[\Delta_{12}]. \quad (26)$$

It has been shown that in the perturbative limit the reconstructions [Eqs. (23), (26), (25)] agree with each other to second order in the interparticle interaction [58].

None of the reconstruction functionals presented above preserves, however, important symmetries of the equations of motion [Eq. (5)], most importantly the contraction consistency (CC). At each instant of time CC requires

$$D_{12}(t) = \frac{1}{N-2} \text{Tr}_3 D_{123}^{\text{R}}(t) \quad (27)$$

to hold. We have recently shown [61,62] that the lack of CC seriously impedes the stability as well as the accuracy of the solutions of the equation of motion of the TD2RDM. This deficiency, however, can be cured for any reconstruction functional [61,62] by way of unitary decomposition of tensors. The unitary decomposition allows to separate any p -particle matrix $M_{j_1 \dots j_p}^{i_1 \dots i_p}$ into basis-invariant components

$$M_{12 \dots p} = M_{12 \dots p; \perp} + M_{12 \dots p; \text{K}}, \quad (28)$$

where $M_{12 \dots p; \text{K}}$ denotes the kernel $M_{12 \dots p; \text{K}}$ under contractions, i.e.,

$$\text{Tr}_p M_{12 \dots p; \text{K}} = 0, \quad (29)$$

while $M_{12 \dots p; \perp}$ denotes the component orthogonal to the kernel. $M_{12 \dots p; \perp}$ carries all the important information encoded in $M_{12 \dots p}$ that survives in the lower-dimensional space upon contraction. In turn, $M_{12 \dots p; \perp}$ can be reconstructed from the information available in the contracted space. Equation (28) applied to the 3RDM yields

$$D_{123} = D_{123; \text{K}} + D_{123; \perp}[D_{12}], \quad (30)$$

with the important consequence that the orthogonal component of D_{123} as well as of Δ_{123} become now exactly known functionals of the 2RDM. This exact functional for three-particle hermitian matrices has been first given in Ref. [61] (see also Refs. [29,79] for a more detailed description). With this decomposition we can now reconstruct parts of the missing components for the above reconstruction functionals

through

$$D_{123}^{\text{R+CC}}[D_{12}] = D_{123; \text{K}}^{\text{R}}[D_{12}] + D_{123; \perp}[D_{12}] \quad (31)$$

or equivalently

$$D_{123}^{\text{R+CC}}[D_{12}] = D_{123}^{\text{R}}[D_{12}] + D_{123; \perp}[D_{12}^{\text{d}}], \quad (32)$$

where the defective part of the 2RDM, D_{12}^{d} , corresponds to the contraction error in the two-particle space

$$D_{12}^{\text{d}} = D_{12} - \frac{1}{N-2} \text{Tr}_3 D_{123}^{\text{R}}. \quad (33)$$

By construction, $D_{123}^{\text{R+CC}}$ is now contraction consistent, i.e.,

$$D_{12} = \frac{1}{N-2} \text{Tr}_3 D_{123}^{\text{R+CC}}[D_{12}]. \quad (34)$$

Equally importantly, the CC correction to D_{123} , $D_{123; \perp}[D_{12}^{\text{d}}]$, provides a correction to the approximate three-particle cumulant

$$\Delta_{123; \perp}[D_{12}] = D_{123; \perp}[D_{12}^{\text{d}}]. \quad (35)$$

In Eq. (35) we have used the fact that the first two terms of the cumulant expansion [Eq. (18)] are already exact functionals of D_{12} . One remarkable consequence of restoring parts of Δ_{123} by the CC correction is that even the Valdemoro approximation whose bare version [Eq. (19)] neglects Δ_{123} entirely contains now in its contraction consistent (V + CC) version a three-particle correlation contribution $\Delta_{123; \perp}$. The residual error for the reconstruction functionals considered can thus be traced to the kernel of the three-particle cumulant $\Delta_{123; \text{K}}$, either completely missing as in the V + CC approximation or only incompletely reconstructed by the NY + CC, TS + CC, or M + CC approximation. In the following, we refer to functionals without the CC correction as the bare functionals.

IV. PROBING THE DYNAMICS OF THE CUMULANTS

The proposed approximate reconstruction functionals for $D_{123}(t)$ or, more specifically, for the three-particle cumulant $\Delta_{123}(t)$ [Eqs. (20), (24), (26)] are at most quadratic functionals in $\Delta_{12}(t)$ and local in time. Higher-order terms in Δ_{12} as well as any memory effects are neglected from the outset. As this simple analytic structure of the approximate reconstruction functionals requires strong temporal correlations between $\Delta_{12}(t)$ and $\Delta_{123}(t)$, it is instructive to probe for the temporal correlations between $\Delta_{123}(t)$ and $\Delta_{12}(t)$ in the exact dynamics of the nonequilibrium few-site Fermi-Hubbard model. Only when such time-correlated dynamics is present within the exact solution, the reconstruction by the time-local reconstruction functionals used here can be expected to be accurate.

For the Fermi-Hubbard model we explore the coupling between $\Delta_{12}(t)$ and $\Delta_{123}(t)$ by following the quench dynamics for varying strength of interparticle correlations (Hubbard parameter U) and strength of the initial out-of-equilibrium excitation (controlled by the confining potential parameter V). We determine the exact time evolution of $\Delta_{12}(t)$ and $\Delta_{123}(t)$ for the quench dynamics without invoking any reconstruction functional. We start from the exact ground state in the potential well of strength V [Fig. 1(a)], which controls the strength of the out-of-equilibrium excitation of the free Fermi-Hubbard

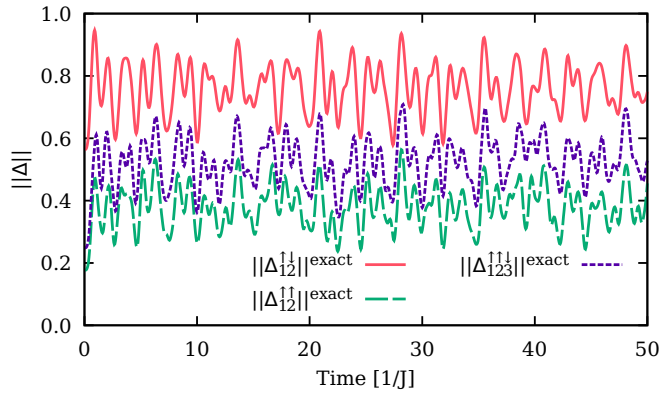


FIG. 4. Time evolution of the exact cumulants (Frobenius norm) for the six-site Fermi-Hubbard model at half-filling after the potential quench with $V = 1J$ and $U = 3.1J$.

model [Fig. 1(b)]. We scan over V in steps of $0.1J$ in the interval $V \in [0.1, 2]J$ and over U in steps of $0.3J$ in the interval $U \in [0.1, 4]J$. (Here and in the following we use the hopping parameter J as characteristic energy scale and $1/J$ as characteristic time scale.) Since in the spin-orbital representation the entire information on Δ_{123} is contained in the spin block $\Delta_{123}^{\uparrow\uparrow\downarrow}$, we focus on the magnitude of $\Delta_{12}^{\uparrow\downarrow}$, $\Delta_{12}^{\uparrow\uparrow}$, and $\Delta_{123}^{\uparrow\uparrow\downarrow}$, as measured by the Frobenius norm (Schatten 2-norm)

$$\|M\| = (\text{Tr}M^\dagger M)^{1/2}. \quad (36)$$

The Frobenius norm provides an upper bound of the largest eigenvalue of M . The square of the Frobenius norm has been used in previous time-dependent studies as a size-extensive measure of correlations [80].

In Fig. 4 we show a typical example for the nonequilibrium dynamics of cumulants at $V = 1J$ and $U = 3.1J$. All cumulants start with nonzero values $\Delta_{12}(t = 0)$ and $\Delta_{123}(t = 0)$ of the initial out-of-equilibrium state. They significantly increase immediately following the potential quench signifying the buildup of dynamical correlations in nonequilibrium dynamics. Direct visual inspection reveals that the variations of $\Delta_{12}^{\uparrow\downarrow}$, $\Delta_{12}^{\uparrow\uparrow}$, and $\Delta_{123}^{\uparrow\uparrow\downarrow}$ are correlated in time with each other. To quantify these time correlations, we calculate the equal-time limit $C_{f,g}(\tau = 0)$ of the normalized cross-correlation function

$$C_{f,g}(\tau) = \frac{\frac{1}{T-t_0} \int_{t_0}^T dt [f(t+\tau) - \bar{f}][g(t) - \bar{g}]}{\sigma_f \sigma_g}, \quad (37)$$

with T the total time interval considered, the standard deviation

$$\sigma_f = \sqrt{\frac{1}{T-t_0} \int_{t_0}^T dt [f(t) - \bar{f}]^2}, \quad (38)$$

and the mean $\bar{f} = \frac{1}{T-t_0} \int_{t_0}^T dt f(t)$ (similarly for g). $C_{f,g}(\tau = 0)$ is also referred to as the Pearson correlation coefficient [81]. With this normalization $-1 \leq C_{f,g}(\tau = 0) \leq 1$ where $C_{f,g}(\tau = 0) = 1(-1)$ corresponds to perfect (anti)correlation and $C_{f,g}(\tau = 0) = 0$ to absence of correlation in time. We use in Eq. (37) a finite lower limit t_0 of the time integral (instead of evaluating the correlation starting with $t = 0$) because the initial rise of the cumulants is always correlated and its

inclusion could lead to an overestimate of the steady-state correlation coefficient. The value of t_0 is found empirically by requiring it to be large enough to separate for most parameters in the U - V plane the initial buildup from the steady-state fluctuations around the mean. The correlation coefficient $C_{f,g}(\tau = 0)$ is designed to characterize only these steady-state fluctuations. For the entire parameter scan we use $t_0 = 10J^{-1}$ and $T = 50J^{-1}$. The behavior of $C_{f,g}(\tau = 0)$ for different cumulant pairs in the U - V plane is displayed in Figs. 5 and 6 for different system sizes (Fig. 5 for $M_s = 6$ sites, Fig. 6 for $M_s = 8$ sites).

To delimit and identify structures in the U - V landscape we introduce two characteristic variables in the U - V plane. One is the ratio of the time-averaged correlation energy \bar{E}_{cor} to the initial degree of excitation parameterized by $E_{\text{pot}}(0)$, $\bar{E}_{\text{cor}}/E_{\text{pot}}(0)$, [Figs. 5(c) and 6(c)]. The latter is given by

$$E_{\text{pot}}(0) = \text{Tr}D_1(t = 0)V_1(t = 0), \quad (39)$$

while

$$E_{\text{cor}}(t) = \text{Tr}_{12}W_{12}\Delta_{12}(t), \quad (40)$$

which in case of the Fermi-Hubbard model reduces to

$$E_{\text{cor}}(t) = U \sum_j \Delta_{j\uparrow j\downarrow}^{\uparrow\downarrow}(t). \quad (41)$$

Another variable measures the buildup of dynamical three-particle correlations during time evolution relative to the three-particle correlations already present in the initial state at $t = 0$ prior to the quench [Figs. 5(d) and 6(d)],

$$\overline{\delta\Delta_{123}^{\uparrow\uparrow\downarrow}} = \frac{1}{T} \int_0^T dt \|\Delta_{123}^{\uparrow\uparrow\downarrow}(t)\| - \|\Delta_{123}^{\uparrow\uparrow\downarrow}(0)\|. \quad (42)$$

The contour line $\overline{\delta\Delta_{123}^{\uparrow\uparrow\downarrow}} = 0.65$ also denoted in Figs. 5(a), 5(b) and 6(a), 6(b) traces quite accurately the borderline between strong and weak time correlation (or anticorrelation) between Δ_{123} and Δ_{12} . We also display the borderline between high and low relative correlation energy by plotting the contour line $\bar{E}_{\text{cor}} = -0.1E_{\text{pot}}(0)$ in Figs. 5(a)–5(c) and 6(a)–6(c), which accurately delimits the region of strong time correlation (i.e., $C_{\Delta_{12}, \Delta_{123}} \lesssim 1$) in the cumulant dynamics.

Obviously, distinct parameter regimes exist for which $\Delta_{123}(t)$ and $\Delta_{12}(t)$ are strongly correlated with each other: one region pertains to small U ($U \lesssim 0.1J$) and a wide range of excitation energies ($0 \leq V \lesssim 2J$), where the cumulants build up over the entire time interval of $T = 50J^{-1}$ and have not reached saturation for most V . This buildup is naturally strongly correlated over the entire time interval. Another prominent region of positive correlations can be associated with negative relative correlation energies $\bar{E}_{\text{cor}} \lesssim -0.1E_{\text{pot}}(0)$ found over the entire interval of U tested and for moderate levels of excitation ($V \lesssim J$). This region is characterized by large amplitude fluctuations with frequencies $\gtrsim J$ an example of which is shown in Fig. 4. In addition we find for the larger system ($M_s = 8$) also a region of time correlation between $\Delta_{12}(t)$ and $\Delta_{123}(t)$ for positive correlation energy of $\bar{E}_{\text{cor}} \gtrsim 0.05E_{\text{pot}}(0)$, which seems to be system specific, as we did not find a similar region for $M_s = 6$ when scanning up to $V = 2.7J$. In this region, all cumulants $\Delta_{12}^{\uparrow\uparrow}$, $\Delta_{12}^{\uparrow\downarrow}$, and

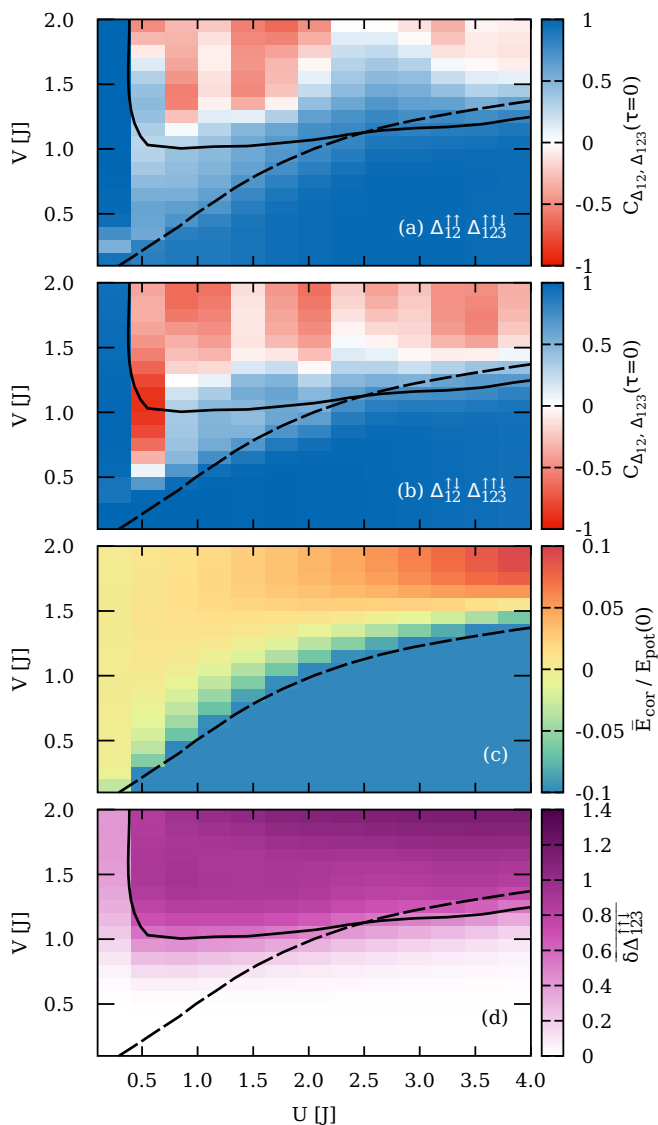


FIG. 5. Six-site Fermi-Hubbard model at half-filling ($M_s = 6$) with interaction U starting from a ground state at varying potential of strength V . Equal-time limit of the normalized cross-correlation function between the three-particle cumulant $\Delta_{123}^{\uparrow\uparrow\downarrow}$ and the two-particle cumulants (a) $\Delta_{12}^{\uparrow\uparrow}$ and (b) $\Delta_{12}^{\uparrow\downarrow}$ in the U - V plane. In (c) we depict the mean (i.e., time-averaged) correlation energy \bar{E}_{cor} relative to the initial excitation energy $E_{pot}(0)$, $\bar{E}_{cor}/E_{pot}(0)$. The color bar is cut below -0.1 (i.e., smaller values than shown on the color bar are present). The black dashed line indicates the contour $\bar{E}_{cor}/E_{pot}(0) = -0.1$. In (d) we show the dynamical buildup of three-particle correlations relative to the initial correlations at $t = 0$, $\overline{\delta\Delta_{123}^{\uparrow\uparrow\downarrow}}$ [Eq. (42)]. The solid black line denotes the $\overline{\delta\Delta_{123}^{\uparrow\uparrow\downarrow}} = 0.65$ contour.

$\Delta_{123}^{\uparrow\uparrow\downarrow}$ initially slowly build up to a large local maximum and subsequently decay to a smaller plateau while fluctuating only with small amplitude around their mean. This predominantly low-frequency dynamics yields small positive values of the normalized correlation coefficient $C_{f,g}(\tau = 0)$ [Eq. (37)].

In view of the quadratic dependence of the approximate reconstruction functionals of $\Delta_{123}(t)$ on $\Delta_{12}(t)$ [Eqs. (20), (24), (26)] the time-correlation maps (Figs. 5 and 6) determined

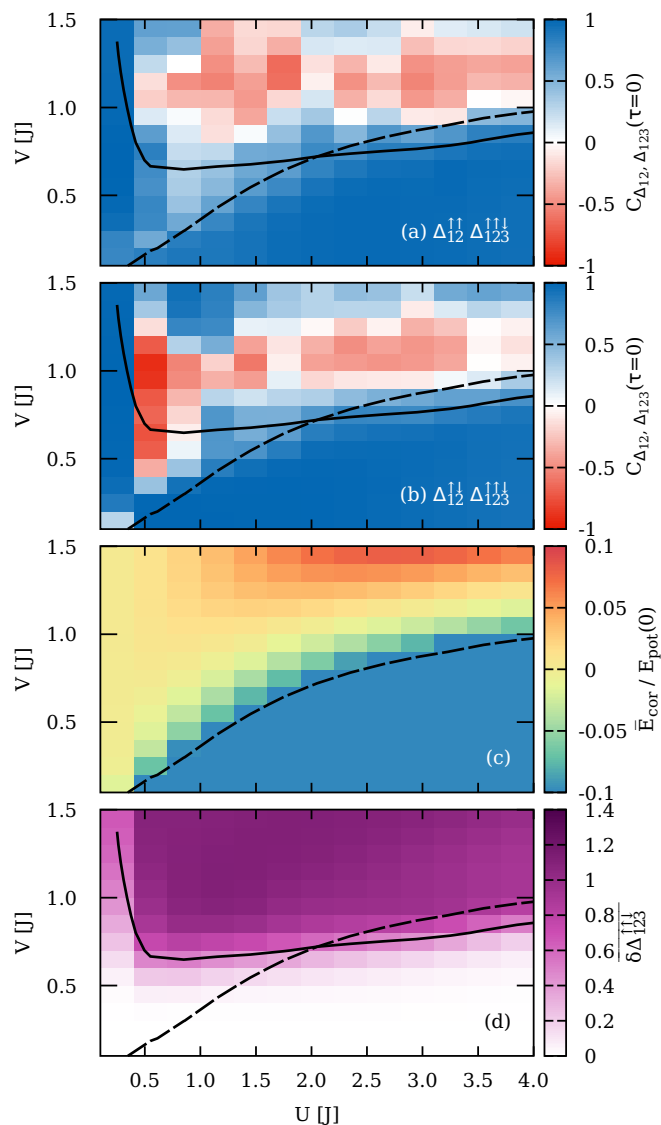


FIG. 6. As in Fig. 5, but for the Fermi-Hubbard model with $M_s = 8$ sites.

here from exact calculations, allow predictions for the anticipated accuracy of the TD2RDM theory. The time evolution of the many-body system should be captured quite well with the present set of reconstruction functionals in those parameter regions in the U - V plane where the time correlation between $\Delta_{12}(t)$ and $\Delta_{123}(t)$ is strong and the buildup of cumulants remains moderate. We therefore anticipate and show below that the reconstruction will be reasonably accurate in regions of positive time correlations as long as the buildup of three-particle correlations over time [Eq. (42)] remains moderate. This is not the case for the additional region of positive correlations for the system with $M_s = 8$, where the Pearson correlation coefficient, being a normalized quantity that is insensitive to the buildup, loses its predictive power.

To assess the accuracy of the reconstruction functionals locally in time and without the accumulation of errors during time evolution, we perform exact calculations of both $D_{12}(t)$ and $D_{123}(t)$ and determine the deviation $\delta D_{123}(t)$ of the reconstructed $D_{123}^R(t)$ from the exact three-particle density matrix

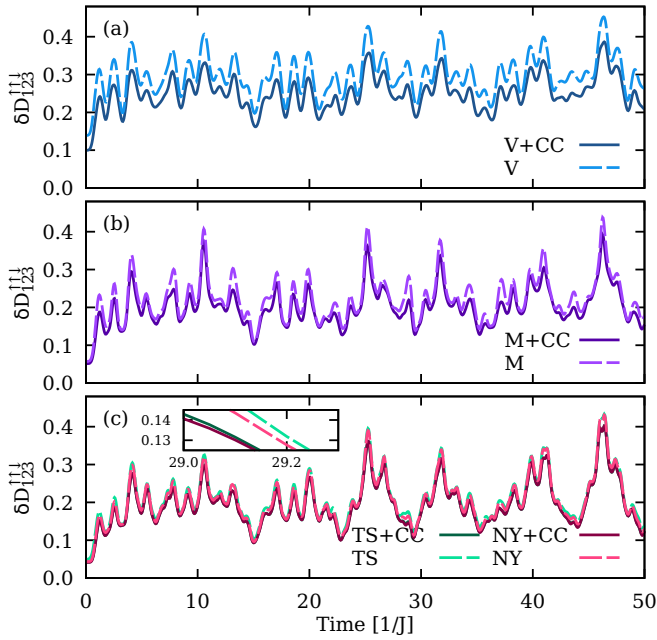


FIG. 7. Six-site Fermi-Hubbard model at half-filling ($M_s = 6$) starting from the many-body ground state in the potential with $V = 0.8J$ defining the out-of-equilibrium initial state in the potential-free Fermi-Hubbard model after the quench. The interaction parameter is $U = 1.9J$. Error in the three-particle reconstruction $\delta D_{123}(t)$ [Eq. (43)] for different reconstruction functionals (a) Valdemoro (V) [Eq. (19)] with and without contraction consistency (CC), (b) Mazzotti (M) [Eq. (26)] with and without CC, and (c) Tohyama-Schuck (TS) [Eq. (25)] and Nakatsuji-Yasuda (NY) [Eq. (23)] with and without CC. The inset in (c) shows a zoom into a region where the differences between TS + CC and NY + CC become visible.

$D_{123}(t)$,

$$\delta D_{123}(t) = \left\| D_{123}^R [D_{12}^{\text{exact}}(t)] - D_{123}^{\text{exact}}(t) \right\|, \quad (43)$$

using the exact $D_{12}(t)$ as input to the reconstruction functional. Taking into account the cumulant expansion of D_{123} [see Eq. (18)] this error coincides with the error in the three-particle cumulant $\delta D_{123}(t) = \delta \Delta_{123}(t)$ as only the latter is subject to reconstruction errors. In Fig. 7 we present exemplary results for $\delta D_{123}(t)$ for the $\Delta_{123}^{\uparrow\uparrow\downarrow}$ block and for the parameters $V = 0.8J$ and $U = 1.9J$ localized in the region of strong temporal correlations [Figs. 5(a) and 5(b)] as well as moderate buildup of three-particle correlations over time [Fig. 5(d)]. As the bare Valdemoro approximation neglects Δ_{123} entirely, its error is largest and corresponds to the exact value of Δ_{123} itself. The bare NY, M, and TS perform better with the NY-reconstruction performing best. The difference between NY and TS is very small indicating that the normalization \mathcal{N} does not play a significant role in this case. Inclusion of the CC corrections improves the performance of all reconstruction functionals (Fig. 7). As expected, the changes are largest for V + CC for which the CC correction given by the orthogonal component of the cumulant, $\Delta_{123;\perp}$ [Eq. (35)], represents the only contribution to Δ_{123} . For the TS and NY functionals, on the other hand, the corrections due to CC are small in this particular case.

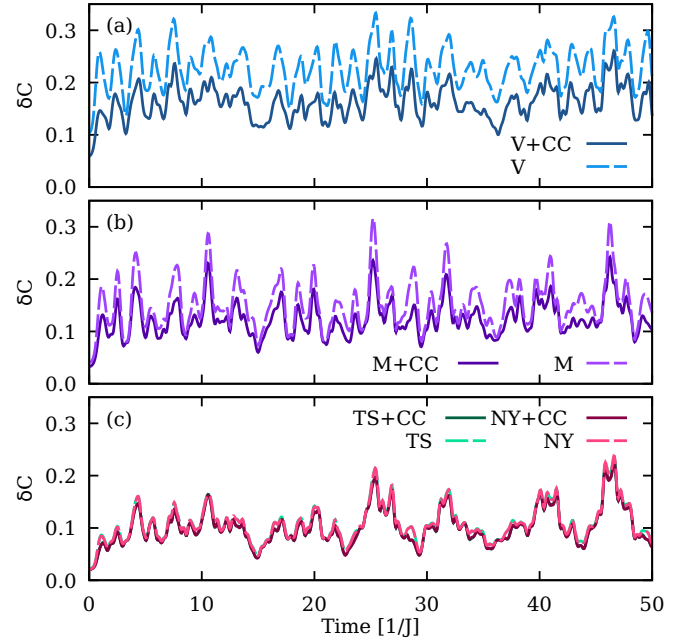


FIG. 8. As in Fig. 7, however for the relative error of the collision operator δC [Eq. (44)].

To further probe the accuracy of the reconstruction functionals within the TD2RDM theory locally in time in more detail we now take into account that only a fraction of the elements of the full 3RDM enters the equations of motion of the 2RDM via the collision operator $C[D_{123}]$ [see Eq. (5)]. We therefore determine the corresponding relative error in the collision operator

$$\delta C(t) = \frac{\left\| C[D_{123}^R(t)] - C_{\text{exact}}(t) \right\|}{\left\| C_{\text{exact}}(t) \right\|}, \quad (44)$$

using the exact input from D_{12}^{exact} in D_{123}^R . The error in the collision operator (shown in Fig. 8 for the $\uparrow\uparrow\downarrow$ block) mirrors closely that of Δ_{123} (Fig. 7). It is largest for the V functional and smallest for the NY + CC functional. In the following benchmark calculations of the nonequilibrium dynamics of the Fermi-Hubbard model we will restrict ourselves to these two functionals, which provide a clear indication of the bandwidth of the expected accuracy.

It is furthermore instructive to directly compare the time-local reconstruction error $\delta D_{123}(t)$ [Eq. (43)] of the V + CC and NY + CC reconstruction functionals for the cumulants with the norm of the cumulants themselves (Fig. 9). Note that the norm $\|\Delta_{123}(t)\|$ [Figs. 9(a) and 9(b)] coincides with the error of the bare V reconstruction functional in which the three-particle is neglected. In turn, the difference to the V + CC functional [Fig. 9(b)] directly indicates the size of $\Delta_{123;\perp}$ included by enforcing contraction consistency. This correction amounts in the present system to an approximate scaling factor of $\approx 0.85 \pm 0.05$. The time-local reconstruction functional NY + CC improves the reconstruction substantially compared to V + CC. We find that NY + CC performs better in regions where $\Delta_{123}^{\uparrow\uparrow\downarrow}$ has local minima but performs similarly as the V + CC in regions of local maxima. This gives an indication

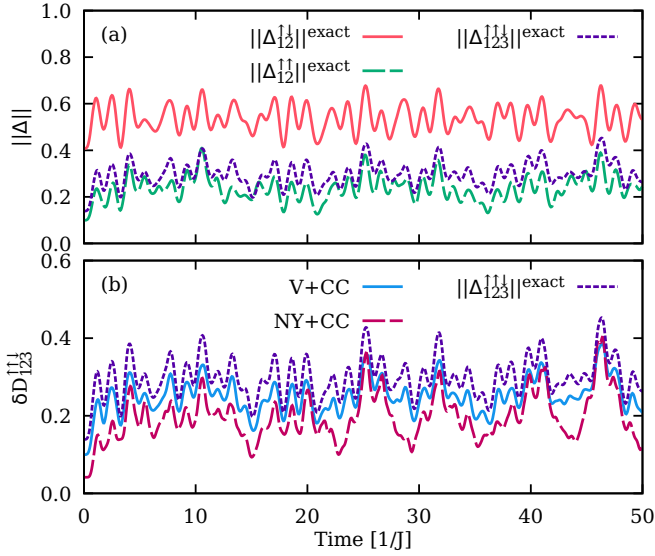


FIG. 9. Same system as in Fig. 7. (a) Dynamics of the two-particle ($\Delta_{12}^{\uparrow\uparrow}$ and $\Delta_{12}^{\uparrow\downarrow}$) and three-particle ($\Delta_{123}^{\uparrow\uparrow\downarrow}$) cumulants as measured by the Frobenius norm and obtained from an exact wavefunction calculation. (b) Time-averaged error of the reconstruction $\delta D_{123}^{\uparrow\uparrow\downarrow}$ using the NY + CC and V + CC functionals compared with $\|\Delta_{123}^{\uparrow\uparrow\downarrow}\|_{\text{exact}}$ [same curve as in (a)].

of current limitations of the reconstruction accuracy and also useful hints for directions of future improvements.

We now analyze the time-averaged reconstruction error in the collision operator [Eq. (44)] in the U - V plane (Fig. 10). The time-averaged error closely mirrors the behavior of the equal-time cross correlation between the two-particle and three-particle cumulants [Eq. (37), Fig. 5]. (The result for $M_s = 8$ looks qualitatively very similar and is omitted for brevity.) For a Fermi-Hubbard system with weak interparticle interactions $U \lesssim 0.1J$ the reconstruction error in the collision operator is very small for both the V + CC and the NY + CC reconstruction. For much larger U of up to $U \approx 3J$ and moderately strong initial excitation ($V \lesssim J$) the NY + CC reconstruction performs markedly better. Remarkably, this region is quite faithfully delimited by the region where the buildup over time of the correlations [Eq. (42)] is moderate, $\delta\Delta_{123}^{\uparrow\uparrow\downarrow} \lesssim 0.65$. Nevertheless, it should be pointed out that the accuracy also of this reconstruction is limited for larger $U \gtrsim 3J$. Interestingly, in the U - V region of time-anticorrelated or uncorrelated dynamics of the cumulants (Figs. 5 and 6), the time-local reconstruction within NY + CC can cause even larger errors than the V + CC. This is not surprising in view of the fact that the V + CC approximation neglects (apart from the CC correction) Δ_{123} entirely and therefore does not enforce time correlations while the NY + CC reconstruction does so through the quadratic dependence of Δ_{123}^{NY} on Δ_{12} [see Eq. (20)]. Also this observation may point to avenues for further improvements of reconstruction functionals.

V. SELF-CONSISTENT PROPAGATION OF THE 2RDM

We present now examples of the fully self-consistent solution of the equations of motion of the 2RDM [Eq. (5)] starting from the pure excited state, the many-body ground state in

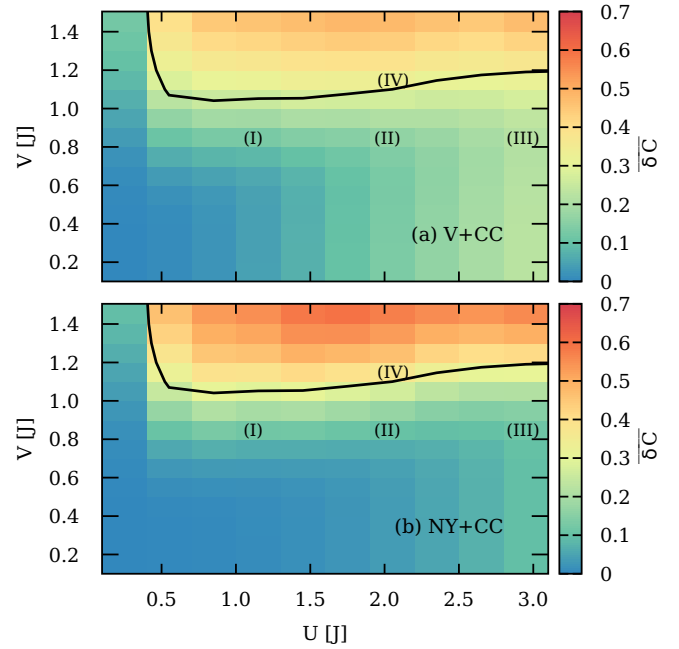


FIG. 10. Six-site Fermi-Hubbard model at half filling ($M_s = 6$) initially ($t = 0$) confined by the harmonic potential of strength V and released for $t > 0$ for varying pair interaction U . Shown is the reconstruction error in the U - V plane measured by the time-averaged relative error of the collision operator $\delta C(t)$ [Eq. (44)] using (a) the V + CC reconstruction functional and (b) the NY + CC reconstruction functional. For the points in the U - V plane marked by Roman numbers (I)–(IV) the time evolution of the occupation numbers $n_1(t)$ is displayed in Fig. 11 and their error in Fig. 12. The black solid line corresponds to the same contour line as in Fig. 5.

the potential $V_i(t)$ prior to the quench at $t = 0$. We present examples of these simulations for different parameters in the U - V plane, as marked in Fig. 10. As observable for the quench dynamics we chose the occupation $n_1(t) = D_1^\dagger(t)$ of the first site. We compare (Fig. 11) the results of the TD2RDM theory for a given reconstruction functional with the corresponding exact calculations. We note that the convergent and accurate propagation of the 2RDM requires, in addition to an accurate three-particle cumulant reconstruction functional, also the preservation of N -representability, which is *a priori* not guaranteed when errors due to the approximate reconstruction functionals pile up. N -representability is approximately restored during propagation by purification on the fly (see Refs. [61,62]). The specific purification algorithm employed in the present simulation is summarized in Appendix C.

The time evolution of $n_1(t)$ for selected values of U and V , marked by Roman numbers in Fig. 10, are displayed for $t \leq 50J^{-1}$ in Fig. 11. For weak on-site interaction $U \lesssim 0.1J$ both the V + CC and the NY + CC reconstruction functionals yield excellent agreement with the exact results over a wide range of out-of-equilibrium excitations $0 \leq V \leq 1.5J$. For stronger U and intermediate quenches with V up to $V = 0.8J$ [Fig. 11 (I)–(III)] we observe excellent agreement for the NY + CC reconstruction which performs better than the V + CC reconstruction. For larger V [e.g., $V = 1.1J$ and $U = 1.9J$, Fig. 11 (IV)] deviations for both functionals from

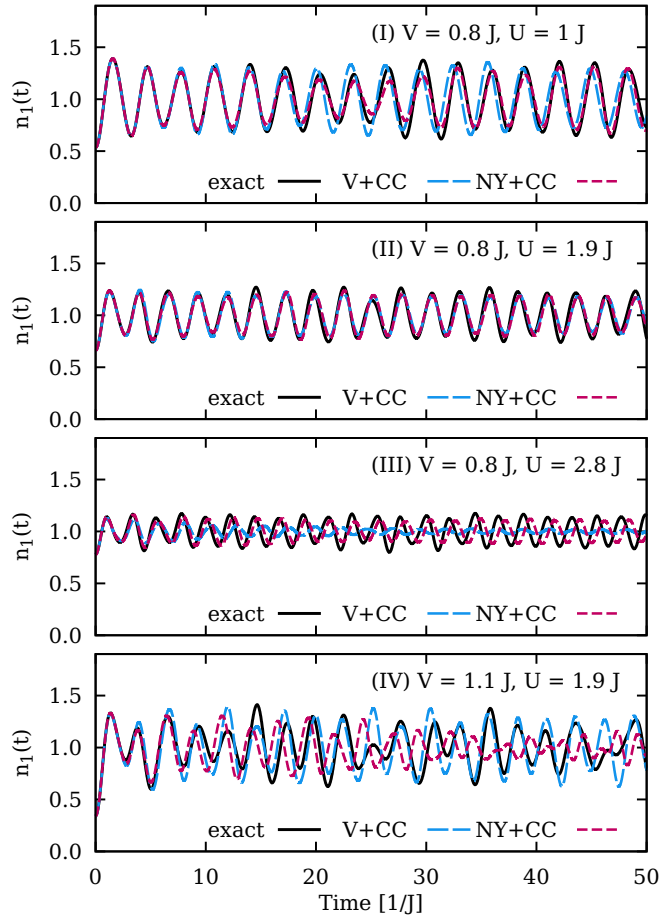


FIG. 11. System as in Fig. 10. Shown is the time evolution of the occupation of site 1, $n_1(t)$ (see Fig. 1) as predicted by TD2RDM using the V + CC and NY + CC functionals and compared with the exact results for different parameter combinations of (U, V) as indicated in the frame and marked in Fig. 10.

the exact result are larger with the V + CC reconstruction functional performing slightly better.

To survey the accuracy of the site occupation $n_1(t)$ in the entire U - V plane we display in Fig. 12 for the six-site Fermi-Hubbard model the time-integrated deviations from the exact result

$$\overline{\delta n_1} = \frac{\int_0^T dt |n_1^{\text{exact}}(t) - n_1(t)|}{\int_0^T dt n_1^{\text{exact}}(t)}, \quad (45)$$

sensitively probing the amplitude, frequency, and phase of the quench-induced density fluctuations. The distribution of $\overline{\delta n_1}$ closely resembles the equal-time correlation between Δ_{12} and Δ_{123} [see Fig. 5, Eq. (37)]. Obviously, the limitation to moderate buildup of three-particle correlations over time ($\delta\Delta_{123}^{\uparrow\uparrow\downarrow} \lesssim 0.65$) is one reliable predictor for accurate long-term simulations of the correlated nonequilibrium dynamics. We emphasize that the present figure of merit ($\overline{\delta n_1} \lesssim 0.1$, i.e., the area shaded green or blue in Fig. 10) puts the theory to a fairly stringent test. Even when $\overline{\delta n_1} \gtrsim 0.3$ the agreement with the exact calculation is qualitatively and even semiquantitatively satisfactory, capturing key features of the fluctuations even though not in all details [see, e.g., Fig. 11 (IV)]. Like-

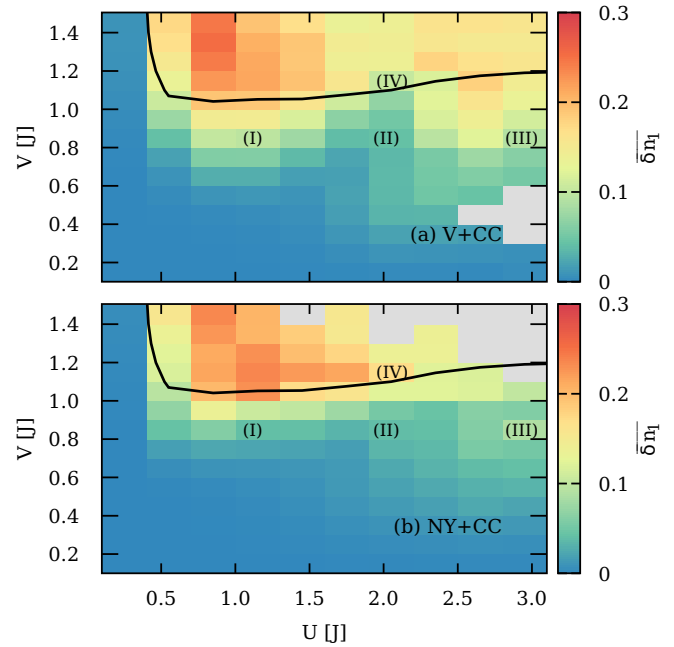


FIG. 12. System as in Fig. 10. Shown is the time-integrated error $\overline{\delta n_1}$ [Eq. (45)] of the occupation number $n_1(t)$ predicted by TD2RDM relative to the exact result in the U - V plane. The black line denotes the $\delta\Delta_{123}^{\uparrow\uparrow\downarrow} = 0.65$ contour of the buildup of three-particle correlations over time [Eq. (42)] (same as in Fig. 5). The gray areas mark regions where the method did not meet the convergence criteria discussed in Appendix C.

wise, when the purification protocol does not fully converge relative to the criteria imposed (see Appendix C), the results for the time-dependent occupation numbers still contain qualitatively correct information on the mean occupation and dominant frequencies.

We now turn to larger systems ($M_s = 18, 20$) and time scales for which exact or highly accurate wave-function-based methods (such as MPSs) are presently still a challenge. We demonstrate here the straightforward applicability of the TD2RDM theory for such systems. For a meaningful comparison with mean-field methods such as TDHF we restrict ourselves to a weakly correlated Fermi-Hubbard model with $U = 0.1J$ but a high degree of excitation. We start with an initial state where all $M_s/2$ sites around the center of the system are doubly occupied amounting to a quench in the limit $V \rightarrow \infty$. For the system size $M_s = 18$ [Fig. 13(a)] we can still compare with exact propagation for the time interval $0 \leq t \leq 80J^{-1}$. For $M_s = 20$ [Fig. 13(b)] we can compare to MPS calculations, which provide a benchmark. The latter are, however, currently limited to short times $t \lesssim 10J^{-1}$ because of the exponential increase in computational effort with time. For $M_s = 18$ we find excellent agreement with the exact results up to $t \approx 60J^{-1}$ and still reasonable agreement for longer times. For $M_s = 20$ we find excellent agreement with the MPS results for the short time interval for which the MPS data could be generated. We emphasize that increasing the system sizes here from $M_s = 18$ to $M_s = 20$ does not pose any major challenge for TD2RDM theory. The extension towards larger systems approaching extended periodic systems thus

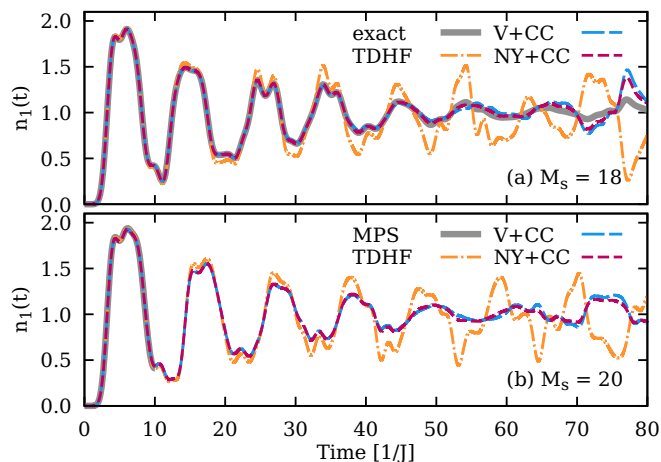


FIG. 13. The Fermi-Hubbard model with (a) $M_s = 18$ sites and (b) $M_s = 20$ sites at half-filling and $U = 0.1J$. All particles are initially located at the center of the system amounting to a potential quench of $V \rightarrow \infty$. The exact solution of the Schrödinger equation in (a) has been obtained using a Trotter decomposition of the sparse time-evolution operator (time step $dt = 0.025J^{-1}$), and via the one-site time-dependent variational principle with matrix product state bond dimension of $\chi = 512$ ($dt = 0.025J^{-1}$) in (b). Convergence with bond dimension and time step has been verified to be within an absolute precision of 10^{-3} for the expectation values shown. We compare with the TD2RDM prediction using the V + CC and NY + CC reconstruction functionals as well as with the mean-field solution within time-dependent Hartree-Fock (TDHF) theory.

appears feasible. We also present in Fig. 13 a comparison with a time-dependent Hartree-Fock (TDHF) simulation as a representative mean-field description within which larger systems are accessible. Even though the system is only weakly correlated, TDHF fails after a short time interval ($t \gtrsim 35J^{-1}$) and substantially overestimates the oscillation amplitude of $n_1(t)$ (Fig. 13). By contrast the TD2RDM method is able to correctly capture the dynamics in this system for extended periods of time.

VI. CONCLUSIONS AND OUTLOOK

In this paper, we have applied the time-dependent two-particle reduced density matrix (TD2RDM) theory to the nonequilibrium dynamics of the finite-size Fermi-Hubbard model at half-filling in one dimension for a wide range of number of sites, interaction strengths U , and initial out-of-equilibrium excitations controlled by the potential strength V of the quench. The Fermi-Hubbard model serves here as a benchmark model to demonstrate the applicability and performance of the theory to extended correlated systems relevant for current research in condensed matter physics and ultracold atoms.

The TD2RDM theory fully incorporates two-particle correlations and includes approximate three-particle correlations via reconstruction functionals. Key to an accurate description of the dynamics within the TD2RDM theory are the reconstruction of the 3RDM, D_{123} , by means of the 2RDM, D_{12} , and application of contraction consistency. The equation of motion of the 2RDM can be closed consistently in this way.

The underlying assumption of the closure is the existence of a sufficiently accurate reconstruction functional of the three-particle cumulant Δ_{123} . The existence of such a reconstruction functional is guaranteed for the ground state via Rosina's theorem [76,77] but its extension to time-dependent settings is currently unknown. Currently used functionals assume Δ_{123} to be local in time, i.e., they do not take into account possible memory effects. By comparing with exact results for small system sizes we have analyzed the dynamics of both two- and three-particle cumulants. Over a wide range of U and V we could identify parameter regimes in which the dynamics of the three-particle and two-particle cumulants are indeed strongly correlated in time with each other, a key prerequisite for the applicability of current state-of-the-art time-local reconstruction functionals. For this particular model system we could show that the TD2RDM theory is applicable and accurate well into the regime of moderately strong correlations ($U \lesssim 3J$), of moderately strong out-of-equilibrium excitations ($V \lesssim J$), and for long propagation times (close to hundred time units J^{-1}). As an approximate parameter controlling the applicability of the TD2RDM theory with the present functionals we could identify the difference $\delta\Delta_{123}$ between the dynamically built up and the initially present (ground-state) three-particle correlations. The importance of temporal correlations between the two- and three-particle cumulants as well as of the buildup of three-particle correlations over time will provide us with directions for further improvements of the reconstruction functionals. Moreover, they may serve as a guidance for the applicability of the TD2RDM theory for systems where exact benchmarks are not available.

Application to larger systems indicates that TD2RDM theory is still capable of providing accurate results and may outperform wave-function-based methods. We have showcased an example in the regime of weak interactions and a high degree of excitation in a system with 18 sites, where a numerically exact solution of the full Schrödinger equation is still possible, and with 20 sites where a MPS solution can be generated, however, only for a limited time span ($\leq 10J^{-1}$). Based on the excellent agreement with these exact results we conclude that the TD2RDM theory has the potential to develop into a versatile tool to study the correlated and strongly driven dynamics of extended models relevant to ultracold atoms and solid-state physics. Application of the TD2RDM theory to extended systems in two and three dimensions is planned.

ACKNOWLEDGMENTS

We thank Daniel Wieser for helpful discussions. I.B. thanks the Simons Foundation for the great hospitality and support during her research visit at the CCQ of the Flatiron Institute. The Flatiron Institute is a division of the Simons Foundation. We acknowledge support from the Max Planck-New York City Center for Non-Equilibrium Quantum Phenomena, Cluster of Excellence 'CUI: Advanced Imaging of Matter' - EXC 2056 - project ID, and the Sub-Auspiciis Award of Excellence of the Austrian Federal Ministry of Education, Science and Research. This research was funded by the WWTF Grant No. MA-14002, the Austrian Science Fund (FWF) grant P 35539-N, the FWF doctoral college

Solids4Fun, as well as the International Max Planck Research School of Advanced Photon Science (IMPRS-APS). Calculations were performed on the Vienna Scientific Cluster (VSC4).

APPENDIX A: EQUATIONS OF MOTION FOR THE 2RDM

We present here the explicit expression for the equation of motion for $D_{j_1 \uparrow j_2 \downarrow}^{i_1 \uparrow i_2 \downarrow}$ in the basis of spin ($\sigma = \uparrow, \downarrow$) orbitals localized at site i , which is obtained from Eq. (5) by inserting Eq. (7) and Eq. (8):

$$\begin{aligned} i\partial_t D_{j_1 \uparrow j_2 \downarrow}^{i_1 \uparrow i_2 \downarrow} &= \sum_n h_n^{i_1} D_{j_1 \uparrow j_2 \downarrow}^{n \uparrow i_2 \downarrow} + \sum_n h_n^{i_2} D_{j_1 \uparrow j_2 \downarrow}^{i_1 \uparrow n \downarrow} \\ &+ U \delta^{i_1, i_2} D_{j_1 \uparrow -j_2 \downarrow}^{i_1 \uparrow i_2 \downarrow} \\ &- \sum_n h_j^n D_{n \uparrow j_2 \downarrow}^{i_1 \uparrow i_2 \downarrow} - \sum_n h_{j_2}^n D_{j_1 \uparrow n \downarrow}^{i_1 \uparrow i_2 \downarrow} \\ &- U \delta_{j_1, j_2} D_{j_1 \uparrow j_2 \downarrow}^{i_1 \uparrow i_2 \downarrow} \\ &+ U D_{i_1 \uparrow j_2 \uparrow j_1 \downarrow}^{i_1 \uparrow i_2 \uparrow i_1 \downarrow} + U D_{j_1 \uparrow i_2 \uparrow j_2 \downarrow}^{i_1 \uparrow i_2 \uparrow i_2 \downarrow} \\ &- U D_{j_1 \uparrow j_2 \uparrow i_1 \downarrow}^{i_1 \uparrow i_2 \uparrow i_1 \downarrow} - U D_{j_1 \uparrow j_2 \uparrow j_2 \downarrow}^{i_1 \uparrow i_2 \uparrow i_2 \downarrow}, \end{aligned} \quad (\text{A1})$$

with

$$h_j^i = -J \delta_j^{i+1} - J \delta_j^{i-1}. \quad (\text{A2})$$

This equation is closed by inserting the reconstructed $D_{j_1 \uparrow j_2 \uparrow j_3 \downarrow}^{i_1 \uparrow i_2 \uparrow i_3 \downarrow}$ [Eq. (9)] into Eq. (A1).

APPENDIX B: MAZZIOTTI RECONSTRUCTION FUNCTIONAL

The Mazziotti reconstruction functional [56] is given in the basis of natural orbitals by

$$\Delta_{j_1 j_2 j_3}^{i_1 i_2 i_3} \text{M} = -\frac{1}{\chi_{j_1 j_2 j_3}^{i_1 i_2 i_3} - 3} \hat{A} \sum_n \Delta_{j_1 j_2}^{i_1 n} \Delta_{n j_3}^{i_2 i_3} \quad (\text{B1})$$

with

$$\chi_{j_1 j_2 j_3}^{i_1 i_2 i_3} = v_{j_1} + v_{j_2} + v_{j_3} + v_{i_1} + v_{i_2} + v_{i_3}, \quad (\text{B2})$$

and v_k the eigenvalues of the 1RDM (i.e., the natural occupation numbers). For propagating the equations of motion in a single-particle basis one has to perform a basis transformation. Elements of the type Δ_{xxx}^{ooo} and Δ_{oou}^{oou} , where o denotes an occupied and u an unoccupied orbital, remain undetermined due to the divergence of the denominator in Eq. (B1) and are chosen to be zero, as suggested in Ref. [56].

APPENDIX C: PURIFICATION

The error through reconstruction of the 3RDM in the equation of motion [Eq. (5)] typically accumulates over time such that the propagation eventually might become unstable [82]. Similar instabilities are found in NEGF methods [29]. We have recently shown [61] that these instabilities can be prevented by enforcing a subset of necessary N -representability conditions during the propagation. N -representability refers to the necessary and sufficient conditions a RDM has to fulfill in order to represent a proper reduction of a fermionic

many-body wave function (or many-body density matrix if ensemble N -representability is concerned) [83]. While for the 1RDM it is sufficient that its eigenvalues lie within the interval $v_i \in [0, 1]$ for ensemble N -representability [84,85], the pure state N -representability problem leads to so-called generalized Pauli constraints [86–89]. For the 2RDM constructive methods exist to obtain a set of necessary ensemble N -representability conditions (see, e.g., Refs. [83,84,90]), but only a limited number of these conditions can be enforced in numerical computations, especially in a time-dependent setting. The problem of sufficient conditions of pure-state N -representability is still widely open [91].

Within the TD2RDM theory, we have shown that enforcing the positive semidefiniteness of the two-particle RDM (D condition) and the corresponding condition on the two-hole RDM,

$$Q_{12} = \hat{A} I_2 - \hat{A} D_1 I_2 + D_{12}, \quad (\text{C1})$$

(the Q condition) is sufficient to stabilize the propagation. Moreover, enforcing the D and Q condition substantially improves the accuracy of all physical observables, even when the equations of motion remain stable. A similar stabilizing effect has been observed within the $G1$ - $G2$ scheme of NEGF methods [29]. In previous studies we have numerically verified that the additional G condition, i.e., the positive-semidefiniteness of the particle-hole RDM, is typically fulfilled when the D and Q conditions are [61].

The present purification protocol enforces positive semidefiniteness of the 2RDM and the two-hole RDM in the least invasive way, which implies preserving their diagonal and off-diagonal traces as well as the energy after each purification step. The relevant diagonal traces are $\sum_n D_{n \uparrow j_2 \downarrow}^{n \uparrow i_2 \downarrow}$ and $\sum_n D_{j_1 \uparrow n \downarrow}^{i_1 \uparrow n \downarrow}$, while the off-diagonal traces read $\sum_n D_{j_1 \uparrow n \downarrow}^{n \uparrow i_2 \downarrow}$ and $\sum_n D_{n \uparrow j_2 \downarrow}^{i_1 \uparrow n \downarrow}$. Our purification protocol utilizes the unitary decomposition of the 2RDM [62]. To this end we determine the component of the 2RDM with negative eigenvalues (i.e., negative geminal occupation numbers) η_i

$$D_{12}^< = \sum_{\eta_i < 0} \eta_i |g_i\rangle \langle g_i|, \quad (\text{C2})$$

and, analogously, the corresponding defective part of the two-hole $Q_{12}^<$. Subtracting these defective parts from D_{12} and Q_{12} would restore a positive semidefinite matrix. However, such a procedure without constraints would lead to violation of conservation of D_1 as well as of the energy. Therefore, we have to enforce in addition

$$\text{Tr}_2 D_{12}^< = 0, \quad (\text{C3})$$

i.e., the subtracted part $D_{12}^<$ must reside in the kernel of the two-particle contraction. Moreover, the two-particle (correlation) energy must be preserved

$$\text{Tr}_{12} W_{12} D_{12}^< = 0. \quad (\text{C4})$$

That part of $D_{12}^<$ meeting these additional requirements Eqs. (C3) and (C4) is denoted by $D_{12}^{<:E}$. We thus arrive at the purification formula for the 2RDM [29]

$$D'_{12} = D_{12} - D_{12;K}^{<:E} - Q_{12;K}^{<:E}, \quad (\text{C5})$$

which we apply iteratively each time the smallest geminal occupation number η_i drops below a preset threshold value. We would like to point out that the results depend only very weakly on the particular threshold value as well as on the maximal number of iterations as long as the iterations converge at all and the smallest geminal occupation number is close to zero (but can still be slightly negative). Since calculating the geminal occupation numbers through exact diagonalization is numerically costly [scaling as $O(M_s^6)$ with the number of sites] we restrict ourselves to applying Eq. (C5) only once each time the smallest geminal occupation number drops below zero for the largest systems in the present paper (with $M_s = 18$ and $M_s = 20$) to save computational time. We have checked that the obtained results are converged with respect to the time step dt of the propagation (i.e., the number of time steps within the entire time interval $[0, T]$). This also means that applying different purification schemes (with respect to the threshold on the smallest geminal occupation number and the number of iterative steps) will give the same results on the level of accuracy set by the threshold.

Reaching numerical convergence as a function of the number of time steps of the propagation when purification is applied poses a challenge in case of large reconstruction errors. We have used an overall global time step dt . However, within each time step we use a time-adaptive propagation (using an explicit Runge-Kutta-Fehlberg propagator of fourth and fifth order) to split each time step into substeps within which the prescribed tolerance of the local error is reached. Whenever the smallest geminal occupation number falls below a certain threshold, purification is applied after the global time step. For the scan in Fig. 12 we have applied a threshold of -10^{-4} and the maximal allowed number of iterations to reach this threshold is set to 100. We observe, however, that there are regions where the iterative purification does not

reach the threshold. These convergence problems occur if either the two-particle cumulant is large already in the initial state, or if it becomes large over time. This can happen in distinct parameter regions. The first region corresponds to the bottom right corner of Fig. 12, i.e., for small V and large $U \gtrsim 3J$, the second region corresponds to large V and $U \gtrsim 0.4J$. Convergence depends also on the reconstruction functional. Correspondingly, we observe that V + CC shows stronger convergence problems in the first region compared to NY + CC, because the cumulant dynamics between the two-particle cumulant and the three-particle cumulant is correlated, and V + CC does not account for this dynamics sufficiently well, leading to larger errors and thus convergence problems during purification [see bottom right corner of Fig. 12(a)]. NY + CC, on the other hand, shows convergence problems in the second region, because the cumulant dynamics is decoupled and NY + CC locally overestimates the three-particle cumulant by using a large two-particle cumulant for reconstruction [see top right corner of Fig. 12(b)]. This does not lead necessarily to instabilities. In fact, we did not observe any instabilities for all values of U and V scanned in Fig. 12. However, frequent applications of purification and large numbers of iterations per purification step may induce undesirable numerical noise. This may prevent convergence as a function of the size of the global time step dt (i.e., as a function of the number of time steps used in the propagation) in cases when the uncontrolled noise accumulates (Fig. 12 gray regions). These areas are identified by a local error in the relevant physical observable (obtained by time-averaging the curves for different global time steps and multiplying by $1/T$) of $>5 \times 10^{-3}$. Even when the simulation does not meet such strict convergence criteria, many observables still appear to be reasonably well represented, e.g., the mean (i.e., time-averaged) occupation number.

-
- [1] A. Pohl, P.-G. Reinhard, and E. Suraud, Towards Single-Particle Spectroscopy of Small Metal Clusters, *Phys. Rev. Lett.* **84**, 5090 (2000).
- [2] M. A. Cazalilla and J. B. Marston, Time-Dependent Density-Matrix Renormalization Group: A Systematic Method for the Study of Quantum Many-Body Out-of-Equilibrium Systems, *Phys. Rev. Lett.* **88**, 256403 (2002).
- [3] J. Caillat, J. Zanghellini, M. Kitzler, O. Koch, W. Kreuzer, and A. Scrinzi, Correlated multi-electron systems in strong laser fields: A multiconfiguration time-dependent Hartree-Fock approach, *Phys. Rev. A* **71**, 012712 (2005).
- [4] T. Burnus, M. A. L. Marques, and E. K. U. Gross, Time-dependent electron localization function, *Phys. Rev. A* **71**, 010501(R) (2005).
- [5] T. Otobe, M. Yamagiwa, J.-I. Iwata, K. Yabana, T. Nakatsukasa, and G. F. Bertsch, First-principles electron dynamics simulation for optical breakdown of dielectrics under an intense laser field, *Phys. Rev. B* **77**, 165104 (2008).
- [6] M. Eckstein, M. Kollar, and P. Werner, Thermalization after an Interaction Quench in the Hubbard Model, *Phys. Rev. Lett.* **103**, 056403 (2009).
- [7] J. A. Driscoll, S. Bubin, and K. Varga, Laser-induced electron emission from nanostructures: A first-principles study, *Phys. Rev. B* **83**, 233405 (2011).
- [8] D. Hochstuhl and M. Bonitz, Time-dependent restricted-active-space configuration-interaction method for the photoionization of many-electron atoms, *Phys. Rev. A* **86**, 053424 (2012).
- [9] D. Hochstuhl, C. M. Hinz, and M. Bonitz, Time-dependent multiconfiguration methods for the numerical simulation of photoionization processes of many-electron atoms, *Eur. Phys. J.: Spec. Top.* **223**, 177 (2014).
- [10] G. Wachter, C. Lemell, J. Burgdörfer, S. A. Sato, X.-M. Tong, and K. Yabana, *Ab Initio* Simulation of Electrical Currents Induced by Ultrafast Laser Excitation of Dielectric Materials, *Phys. Rev. Lett.* **113**, 087401 (2014).
- [11] T. Sato, H. Pathak, Y. Orimo, and K. L. Ishikawa, Communication: Time-dependent optimized coupled-cluster method for multielectron dynamics, *J. Chem. Phys.* **148**, 051101 (2018).
- [12] T. B. Pedersen and S. Kvaal, Symplectic integration and physical interpretation of time-dependent coupled-cluster theory, *J. Chem. Phys.* **150**, 144106 (2019).

- [13] G. E. Topp, N. Tancogne-Dejean, A. F. Kemper, A. Rubio, and M. A. Sentef, All-optical nonequilibrium pathway to stabilizing magnetic Weyl semimetals in pyrochlore iridates, *Nature Commun.* **9**, 4452 (2018).
- [14] M. Buzzi, G. Jotzu, A. Cavalleri, J. I. Cirac, E. A. Demler, B. I. Halperin, M. D. Lukin, T. Shi, Y. Wang, and D. Podolsky, Higgs-Mediated Optical Amplification in a Nonequilibrium Superconductor, *Phys. Rev. X* **11**, 011055 (2021).
- [15] L. Stojchevska, I. Vaskivskiy, T. Mertelj, P. Kusar, D. Svetin, S. Brazovskii, and D. Mihailovic, Ultrafast switching to a stable hidden quantum state in an electronic crystal, *Science* **344**, 177 (2014).
- [16] N. Schlünzen, S. Hermanns, M. Bonitz, and C. Verdozzi, Dynamics of strongly correlated fermions: Ab initio results for two and three dimensions, *Phys. Rev. B* **93**, 035107 (2016).
- [17] C. Giannetti, M. Capone, D. Fausti, M. Fabrizio, F. Parmigiani, and D. Mihailovic, Ultrafast optical spectroscopy of strongly correlated materials and high-temperature superconductors: a non-equilibrium approach, *Adv. Phys.* **65**, 58 (2016).
- [18] K. Balzer, M. R. Rasmussen, N. Schlünzen, J.-P. Joost, and M. Bonitz, Doublon Formation by Ions Impacting a Strongly Correlated Finite Lattice System, *Phys. Rev. Lett.* **121**, 267602 (2018).
- [19] D. N. Basov, A. Asenjo-Garcia, P. J. Schuck, X. Zhu, and A. Rubio, Polariton panorama, *Nanophotonics* **10**, 549 (2020).
- [20] D. M. Kennes, M. Claassen, L. Xian, A. Georges, A. J. Millis, J. Hone, C. R. Dean, D. N. Basov, A. N. Pasupathy, and A. Rubio, Moiré heterostructures as a condensed-matter quantum simulator, *Nature Phys.* **17**, 155 (2021).
- [21] M. Budden, T. Gebert, M. Buzzi, G. Jotzu, E. Wang, T. Matsuyama, G. Meier, Y. Laplace, D. Pontiroli, M. Riccò, F. Schlawin, D. Jaksch, and A. Cavalleri, Evidence for metastable photo-induced superconductivity in K3C60, *Nature Phys.* **17**, 611 (2021).
- [22] A. Niggas, J. Schwestka, K. Balzer, D. Weichselbaum, N. Schlünzen, R. Heller, S. Creutzburg, H. Inani, M. Tripathi, C. Speckmann, N. McEvoy, T. Susi, J. Kotakoski, Z. Gan, A. George, A. Turchanin, M. Bonitz, F. Aumayr, and R. A. Wilhelm, Ion-Induced Surface Charge Dynamics in Freestanding Monolayers of Graphene and MoS₂ Probed by the Emission of Electrons, *Phys. Rev. Lett.* **129**, 086802 (2022).
- [23] J. Bloch, A. Cavalleri, V. Galitski, M. Hafezi, and A. Rubio, Strongly correlated electron-photon systems, *Nature (London)* **606**, 41 (2022).
- [24] J. Zanghellini, M. Kitzler, C. Fabian, T. Brabec, and A. Scrinzi, An MCTDHF approach to multielectron dynamics in laser fields, *Laser Physics-Lawrence* **13**, 1064 (2003).
- [25] J. Haegeman, J. I. Cirac, T. J. Osborne, I. Pižorn, H. Verschelde, and F. Verstraete, Time-Dependent Variational Principle for Quantum Lattices, *Phys. Rev. Lett.* **107**, 070601 (2011).
- [26] A. J. Daley, C. Kollath, U. Schollwöck, and G. Vidal, Time-dependent density-matrix renormalization-group using adaptive effective Hilbert spaces, *J. Stat. Mech.* (2004) P04005.
- [27] C. Kollath, U. Schollwöck, and W. Zwerger, Spin-Charge Separation in Cold Fermi Gases: A Real Time Analysis, *Phys. Rev. Lett.* **95**, 176401 (2005).
- [28] N. Schlünzen, J.-P. Joost, F. Heidrich-Meisner, and M. Bonitz, Nonequilibrium dynamics in the one-dimensional fermi-hubbard model: Comparison of the nonequilibrium Green-functions approach and the density matrix renormalization group method, *Phys. Rev. B* **95**, 165139 (2017).
- [29] J.-P. Joost, N. Schlünzen, H. Ohldag, M. Bonitz, F. Lackner, and I. Březinová, Dynamically screened ladder approximation: Simultaneous treatment of strong electronic correlations and dynamical screening out of equilibrium, *Phys. Rev. B* **105**, 165155 (2022).
- [30] J. Haegeman, C. Lubich, I. Oseledets, B. Vandereycken, and F. Verstraete, Unifying time evolution and optimization with matrix product states, *Phys. Rev. B* **94**, 165116 (2016).
- [31] B. Kloss, Y. B. Lev, and D. Reichman, Time-dependent variational principle in matrix-product state manifolds: Pitfalls and potential, *Phys. Rev. B* **97**, 024307 (2018).
- [32] M. Yang and S. R. White, Time-dependent variational principle with ancillary krylov subspace, *Phys. Rev. B* **102**, 094315 (2020).
- [33] E. Runge and E. K. U. Gross, Density-Functional Theory for Time-Dependent Systems, *Phys. Rev. Lett.* **52**, 997 (1984).
- [34] C. A. Ullrich, *Time Dependent Density Functional Theory* (Oxford University Press, Oxford, 2012).
- [35] G. Vignale and W. Kohn, Current-Dependent Exchange-Correlation Potential for Dynamical Linear Response Theory, *Phys. Rev. Lett.* **77**, 2037 (1996).
- [36] R. D'Agosta and G. Vignale, Relaxation in Time-Dependent Current-Density-Functional Theory, *Phys. Rev. Lett.* **96**, 016405 (2006).
- [37] J. W. Furness *et al.*, Current density functional theory using meta-generalized gradient exchange-correlation functionals, *J. Chem. Theory Comput.* **11**, 4169 (2015).
- [38] K. Pernal, O. Gritsenko, and E. J. Baerends, Time-dependent density-matrix-functional theory, *Phys. Rev. A* **75**, 012506 (2007).
- [39] K. J. H. Giesbertz, E. J. Baerends, and O. V. Gritsenko, Charge Transfer, Double and Bond-Breaking Excitations with Time-Dependent Density Matrix Functional Theory, *Phys. Rev. Lett.* **101**, 033004 (2008).
- [40] K. J. H. Giesbertz, O. V. Gritsenko, and E. J. Baerends, Response Calculations with an Independent Particle System with an Exact One-Particle Density Matrix, *Phys. Rev. Lett.* **105**, 013002 (2010).
- [41] K. Huang, *Statistical Mechanics*, 2nd ed. (New York, Wiley, 2008).
- [42] M. Bonitz, *Quantum Kinetic Theory*, 2nd ed. (Springer International Publishing, Berlin, 2015).
- [43] L. V. Keldysh, Diagram technique for nonequilibrium processes, *Sov. Phys. JETP* **20**, 1018 (1965).
- [44] G. Stefanucci and R. van Leeuwen, *Nonequilibrium Many-Body Theory of Quantum Systems: A Modern Introduction* (Cambridge University Press, Cambridge, 2013).
- [45] N. Schlünzen, S. Hermanns, M. Scharnke, and M. Bonitz, Ultrafast dynamics of strongly correlated fermions—nonequilibrium Green functions and selfenergy approximations, *J. Phys.: Condens. Matter* **32**, 103001 (2020).
- [46] N. Schlünzen, J.-P. Joost, and M. Bonitz, Achieving the Scaling Limit for Nonequilibrium Green Functions Simulations, *Phys. Rev. Lett.* **124**, 076601 (2020).
- [47] D. Karlsson, R. van Leeuwen, Y. Pavlyukh, E. Perfetto, and G. Stefanucci, Fast Green's Function Method for Ultrafast Electron-Boson Dynamics, *Phys. Rev. Lett.* **127**, 036402 (2021).

- [48] Y. Pavlyukh, E. Perfetto, D. Karlsson, R. van Leeuwen, and G. Stefanucci, Time-linear scaling nonequilibrium Green's function methods for real-time simulations of interacting electrons and bosons. I. Formalism, *Phys. Rev. B* **105**, 125134 (2022).
- [49] D. A. Mazziotti, Realization of Quantum Chemistry without Wave Functions through First-Order Semidefinite Programming, *Phys. Rev. Lett.* **93**, 213001 (2004).
- [50] D. A. Mazziotti, Variational reduced-density-matrix method using three-particle N -representability conditions with application to many-electron molecules, *Phys. Rev. A* **74**, 032501 (2006).
- [51] J. R. Hammond and D. A. Mazziotti, Variational reduced-density-matrix calculation of the one-dimensional Hubbard model, *Phys. Rev. A* **73**, 062505 (2006).
- [52] A. E. DePrince and D. A. Mazziotti, Parametric approach to variational two-electron reduced-density-matrix theory, *Phys. Rev. A* **76**, 042501 (2007).
- [53] M. Nakata, B. J. Braams, K. Fujisawa, M. Fukuda, J. K. Percus, M. Yamashita, and Z. Zhao, Variational calculation of second-order reduced density matrices by strong N -representability conditions and an accurate semidefinite programming solver, *J. Chem. Phys.* **128**, 164113 (2008).
- [54] F. Colmenero, C. Pérez del Valle, and C. Valdemoro, Approximating q -order reduced density matrices in terms of the lower-order ones. I. General relations, *Phys. Rev. A* **47**, 971 (1993).
- [55] K. Yasuda and H. Nakatsuji, Direct determination of the quantum-mechanical density matrix using the density equation. II., *Phys. Rev. A* **56**, 2648 (1997).
- [56] D. A. Mazziotti, Pursuit of N -representability for the contracted Schrödinger equation through density-matrix reconstruction, *Phys. Rev. A* **60**, 3618 (1999).
- [57] D. A. Mazziotti, Complete reconstruction of reduced density matrices, *Chem. Phys. Lett.* **326**, 212 (2000).
- [58] A. E. DePrince and D. A. Mazziotti, Cumulant reconstruction of the three-electron reduced density matrix in the anti-Hermitian contracted Schrödinger equation, *J. Chem. Phys.* **127**, 104104 (2007).
- [59] M. Tohyama and P. Schuck, Truncation scheme of time-dependent density-matrix approach II, *Eur. Phys. J. A* **53**, 186 (2017).
- [60] M. Tohyama and P. Schuck, Truncation scheme of time-dependent density-matrix approach III, *Eur. Phys. J. A* **55**, 74 (2019).
- [61] F. Lackner, I. Březinová, T. Sato, K. L. Ishikawa, and J. Burgdörfer, Propagating two-particle reduced density matrices without wave functions, *Phys. Rev. A* **91**, 023412 (2015).
- [62] F. Lackner, I. Březinová, T. Sato, K. L. Ishikawa, and J. Burgdörfer, High-harmonic spectra from time-dependent two-particle reduced-density-matrix theory, *Phys. Rev. A* **95**, 033414 (2017).
- [63] E. Haller, J. Hudson, A. Kelly, D. A. Cotta, B. Peaudecerf, G. D. Bruce, and S. Kuhr, Single-atom imaging of fermions in a quantum-gas microscope, *Nature Phys.* **11**, 738 (2015).
- [64] D. Greif, M. F. Parsons, A. Mazurenko, C. S. Chiu, S. Blatt, F. Huber, G. Ji, and M. Greiner, Site-resolved imaging of a fermionic Mott insulator, *Science* **351**, 953 (2016).
- [65] M. F. Parsons, F. Huber, A. Mazurenko, C. S. Chiu, W. Setiawan, K. Wooley-Brown, S. Blatt, and M. Greiner, Site-Resolved Imaging of Fermionic Li 6 in an Optical Lattice, *Phys. Rev. Lett.* **114**, 213002 (2015).
- [66] L. W. Cheuk, M. A. Nichols, M. Okan, T. Gersdorf, V. V. Ramasesh, W. S. Bakr, T. Lompe, and M. W. Zwierlein, Quantum-Gas Microscope for Fermionic Atoms, *Phys. Rev. Lett.* **114**, 193001 (2015).
- [67] L. W. Cheuk, M. A. Nichols, K. R. Lawrence, M. Okan, H. Zhang, E. Khatami, N. Trivedi, T. Paiva, M. Rigol, and M. W. Zwierlein, Observation of spatial charge and spin correlations in the 2D Fermi-Hubbard model, *Science* **353**, 1260 (2016).
- [68] C. S. Chiu, G. Ji, A. Mazurenko, D. Greif, and M. Greiner, Quantum State Engineering of a Hubbard System with Ultracold Fermions, *Phys. Rev. Lett.* **120**, 243201 (2018).
- [69] J. Eisert, M. Friesdorf, and C. Gogolin, Quantum many-body systems out of equilibrium, *Nat. Phys.* **11**, 124 (2015).
- [70] S. Hermanns, N. Schülzen, and M. Bonitz, Hubbard nanoclusters far from equilibrium, *Phys. Rev. B* **90**, 125111 (2014).
- [71] C. Bertrand, O. Parcollet, A. Maillard, and X. Waintal, Quantum Monte Carlo algorithm for out-of-equilibrium Green's functions at long times, *Phys. Rev. B* **100**, 125129 (2019).
- [72] C. Bertrand, S. Florens, O. Parcollet, and X. Waintal, Reconstructing Nonequilibrium Regimes of Quantum Many-Body Systems from the Analytical Structure of Perturbative Expansions, *Phys. Rev. X* **9**, 041008 (2019).
- [73] Y. Núñez Fernández, M. Jeannin, P. T. Dumitrescu, T. Kloss, J. Kaye, O. Parcollet, and X. Waintal, Learning Feynman Diagrams with Tensor Trains, *Phys. Rev. X* **12**, 041018 (2022).
- [74] I. Bloch and J. Dalibard and S. Nascimbène, Quantum simulations with ultracold quantum gases, *Nature Phys.* **8**, 267 (2012).
- [75] W. Kutzelnigg and D. Mukherjee, Cumulant expansion of the reduced density matrices, *J. Chem. Phys.* **110**, 2800 (1999).
- [76] M. Rosina, *Reduced Density Operators with Application to Physical, Chemical Systems* (Springer, Ontario, 1968).
- [77] D. Mazziotti, *Advances in Chemical Physics: Volume 134: Reduced-Density-Matrix Mechanics. With Application to Many-Electron Atoms and Molecules* (Wiley, New York, 2007).
- [78] S.-J. Wang and W. Cassing, Explicit treatment of N -body correlations within a density-matrix formalism, *Ann. Phys. (NY)* **159**, 328 (1985).
- [79] F. Lackner, Ph.D. thesis, TU Wien, 2017, <https://doi.org/10.34726/hss.2017.39160>.
- [80] J. T. Skolnik and D. A. Mazziotti, Cumulant reduced density matrices as measures of statistical dependence and entanglement between electronic quantum domains with application to photosynthetic light harvesting, *Phys. Rev. A* **88**, 032517 (2013).
- [81] K. Pearson, VII. Mathematical contributions to the theory of evolution.—III. Regression, heredity, and panmixia, *Philos. Trans. R. Soc. Lond. A* **187**, 253 (1896).
- [82] A. Akbari, M. J. Hashemi, A. Rubio, R. M. Nieminen, and R. van Leeuwen, Challenges in truncating the hierarchy of time-dependent reduced density matrices equations, *Phys. Rev. B* **85**, 235121 (2012).
- [83] C. Garrod and J. K. Percus, Reduction of the N -Particle Variational Problem, *J. Math. Phys.* **5**, 1756 (1964).
- [84] A. J. Coleman, Structure of fermion density matrices, *Rev. Mod. Phys.* **35**, 668 (1963).
- [85] R. G. Parr and W. Yang, *Density Functional Theory of Atoms and Molecules* (Oxford University Press, New York, 1989).

- [86] A. A. Klyachko, Quantum marginal problem and N -representability, *J. Phys.: Conf. Ser.* **36**, 72 (2006).
- [87] M. Altunbulak and A. Klyachko, The pauli principle revisited, *Commun. Math. Phys.* **282**, 287 (2008).
- [88] C. Schilling, D. Gross, and M. Christandl, Pinning of Fermionic Occupation Numbers, *Phys. Rev. Lett.* **110**, 040404 (2013).
- [89] C. Schilling, M. Altunbulak, S. Knecht, A. Lopes, J. D. Whitfield, M. Christandl, D. Gross, and M. Reiher, Generalized Pauli constraints in small atoms, *Phys. Rev. A* **97**, 052503 (2018).
- [90] D. A. Mazziotti, Structure of Fermionic Density Matrices: Complete N -Representability Conditions, *Phys. Rev. Lett.* **108**, 263002 (2012).
- [91] P. W. Ayers and E. R. Davidson, Necessary conditions for the N -representability of pair distribution functions, *Int. J. Quantum Chem.* **106**, 1487 (2006).